Proceedings of the
8th ENIGMA meeting

6 - 8 September 2006, Espoo, Finland

T. Hovatta, E. Nieppola, I. Torniainen (editors)

Organized by the Metsähovi Radio Observatory team

Foreword

The 8th and last meeting of the European Network for the Investigation of Galactic nuclei through Multifrequency Analysis (ENIGMA, http://www.lsw.uni-heidelberg.de/projects/enigma/) was held 6 – 8 September in Espoo Finland. In this publication we present the proceedings of the meeting. Writing a proceedings paper was optional, so this compilation is only a cross section of all the research topics discussed by the participants. The papers offer an overview of some of the research projects within ENIGMA. At the end of the network, we wish to thank not only the participants of the 8th meeting, but all the people who have been involved in ENIGMA during the years.

Kirkkonummi 30 October 2006

The Local Organizing Committee

Contents

ENIGMA - European Network for
the Investigation of Galactic nuclei
through Multifrequency Analysis
Proceedings of the 8th Meeting
Sept. 2006, Espoo, Finland

Highlights of the first XMM-Newton observations of OJ 287 and coordinated multiwavelength campaign

Stefano Ciprini[1,2]
(on behalf of people collaborating in this campaign)

[1] Physics Department, University of Perugia, and INFN Perugia Section, via Pascoli, 06123 Perugia, Italy
e-mail: stefano.ciprini@pg.infn.it

[2] Tuorla Observatory, University of Turku, Väisäläntie 20, 21500 Piikkiö, Finland

Abstract. One of the aims of the European Network for the Investigation of Galactic nuclei through Multifrequency Analysis (ENIGMA), was the organization and implementation of international multiwavelength campaigns, exploiting space-borne and ground-based astrophysical facilities, and the development of blazar multifrequency analysis and modelling. A short summary of a campaign devoted to the peculiar blazar OJ 287 is reported here, as one of the main activity performed during the recruitment of the author in this Research Network. X-ray data obtained during the two proposed XMM-Newton observations of OJ 287 in 2005, showed different brightness states and different spectral slopes and components. The X-ray observation epochs corresponded also to two active and flaring stages at optical wavelengths.

Key words. Blazars: general – BL Lacertae objects: individual: OJ 287 – X-rays: galaxies – Radiation mechanisms: non-thermal – Methods: observational

1. Introduction

ENIGMA is the acronym of the European Network for the Investigation of Galactic nuclei through Multifrequency Analysis, a network funded by the European Commission through the Training and Mobility for Researchers (TMR) programme. The Network program combined new strategies in empirical and theoretical research aimed towards an understanding of the structure and acceleration/radiation processes in blazars. One of the main topics of the Network Teams was the organization and implementation of international multiwavelength (MW) campaigns, and the development of analysis/modelling able to explain the MW data obtained during these observing projects. Several coordinated MW monitoring programmes and

Source	Other name	Redshift	EGRET detection	X-rays past observations	X-ray integral flux [erg cm^{-2} s^{-1}]	Optical visibility window
OJ 287	PKS 0851+202	$z = 0.306$	YES (5σ)	Einstein,EXOSAT,ROSAT	1.8, 2.5 $\times 10^{-12}$ (2-10 keV)	Oct.-May
	PG 0851+202			ASCA,*Beppo*SAX	(XMM, Apr., Nov. 2005)	
	1ES 0851+203			XMM (AO-4, AO-5, S.Ciprini)		

Fig. 1. Basic characteristics and the existing X-ray observations of OJ 287.

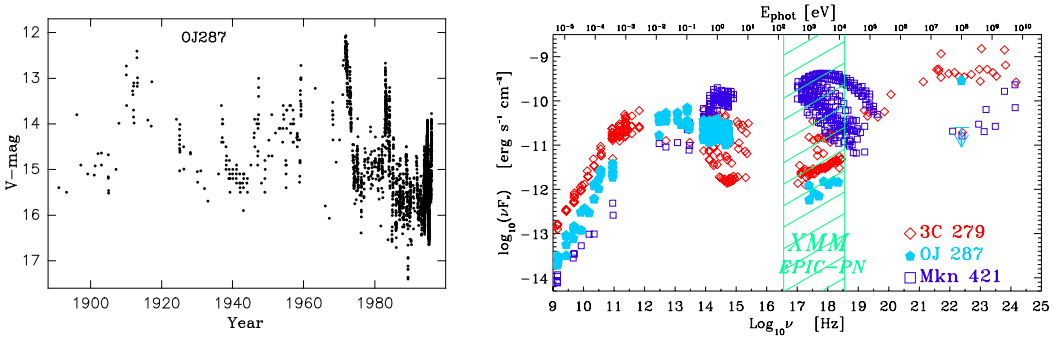

Fig. 2. *Left panel*: the popular historical (1891-2003) optical light curve of OJ 287. *Right panel*: the overall spectral energy distribution (SED) of OJ 287 (a typical low energy peaked BL Lac object, LBL, filled symbols) in comparison with the overall SEDs of 3C 279 (a typical flat-spectrum radio quasar, FSRQ), and Mkn 421 (a typical high-energy peaked BL Lac object, HBL).

MW campaigns on specific blazars were organized exploiting space-borne and ground-based astrophysical facilities and instruments. A short summary on a campaign devoted to the peculiar blazar OJ 287 is reported here, as one of the main activities performed by the author during his recruitment in this Research Network.

2. OJ 287

Blazars (BL Lac objects and high-polarization/flat-spectrum radio quasars) are a class of AGN showing usually high energy radiation and exhibiting rapid and intense flux variations on different timescales at all the wavelengths, from radio to γ-rays. The accepted scenario assumes a supermassive black hole surrounded by an accretion disc, feeding an accelerated–radiating plasma jet, closely oriented to the line of sight, and thus observed as strongly affected by relativistic Doppler beaming effects.

OJ 287 (PKS 0851+202, PG 0851+202, $z = 0.306$) is the only known extragalactic source showing convincing hints of a major periodical trend in its optical emission (roughly a 12 year recurrence). Some models suggest periodic outburst due to the binary nature of the central engine (Nilsson et al. 2006; Valtonen et al. 2006a; Valtonen et al. 2006b;
Valtaoja et al. 2000; Sillanpää et al. 1996; Lehto & Valtonen 1996). Despite the poor evidence, supermassive black holes should appear in binary pairs in a fair number of AGN.

OJ 287 is also a highly-variable (optical variation > 3 mag) and low-energy peaked BL Lac object (LBL), observed and monitored by many years in radio-optical bands. In particular historical optical data are available since 1891. This blazar and MW observing campaigns devoted to it are thus important mainly for two reasons. This AGN is peculiar showing possible periodical behaviour and implications for binary supermassive black holes scenarios.

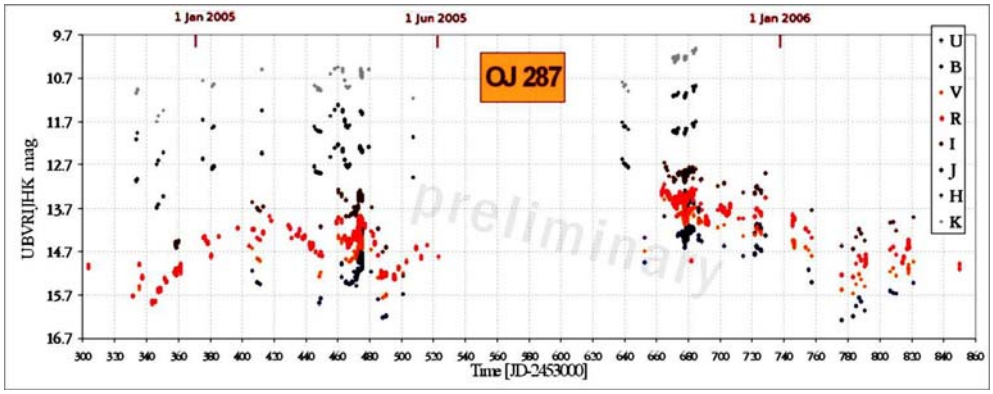

Fig. 3. The whole optical and near-infrared dataset of the coordinated and extended ENIGMA campaign on OJ 287, triggered by the 2 XMM-Newton pointings in 2005. This "multicolour" light curve covers the period October 2004 - April 2006, and has been obtained by more than 30 ground-based observatories. Intensive-observation data of about 1 week around the first satellite pointing date in April 2005, and from about 20 days around the second satellite pointing date in November 2005 belongs to the international consortium WEBT (involved to obtain a more intensive sampling in the coordinated observation). Data from other parallel long-term monitoring programmes and observing projects in this 1.5 year period (covering 2 observing seasons), will possibly provide a better sampling of such light curve.

Secondly the available extensive and long-term data (see, e.g. Fig. 2), allows a comprehensive analysis of the evolution on different timescales.

3. The XMM-Newton coordinated campaign

OJ 287 as a typical LBL shows a double-bump in the overall SED, where the lower energy component (due to synchrotron emission) spans from the radio to the UV bands, while the high energy component (possibly due to inverse Compton, IC scattering) ranges from the X-rays to γ-rays (Fig. 2). OJ 287 is a γ-ray emitting blazar (Shrader et al. 1996), while past X-ray observations were performed by Einstein, EXOSAT, ROSAT, ASCA, *Beppo*SAX (Fig. 1). Proposed GO observation by XMM-Netwon were awarded in 3 occasions. AO-4, 2 pointings in Apr.12, 2005 and Nov.3-4, 2005. The 3^{rd} (AO-5) pointing is scheduled in the next Nov.17, 2006.

The main goals of the XMM-Newton observations and coordinated MW (short/intensive and long-term) campaign can be summarized as the following:

- to observe and study the spectral and temporal behaviour of OJ 287 on both short and long time scales, using long-term monitoring data (mainly radio and optical observations), and some simultaneous, intensive and short-duration MW outlooks (radio, mm, IR, optical, UV and X-ray bands);
- to observe and study the spectral and temporal behaviour of OJ 287 possibly before and during the next foreseen large outburst, in different brightness states (e.g. during quiescence and faint states, during non-thermal flares, during outbursts possibly related to the binary black-hole paradigm).
- to provide information on the high-energy emission component of the SED, and on possible spectral breaks (disentangling different emission components like the synchrotron and inverse Compton, IC, mechanisms) thanks to

the X-ray spectral information provided by the EPIC instrument on board of XMM-Newton;
- to provide simultaneous data on the UV emission of OJ 287 thanks to the OM instrument on board of XMM-Newton;
- to search for and analyze MW correlations in the source;
- to provide useful data in the study of the connection between the X-ray flux and the observed VLBA/VLBI radio structure;
- to challenge for the first time a satellite-triggered and coordinated MW campaign.

This strategy allows to cover a large range of variability timescales (short/long), and a wide range of electromagnetic frequencies, providing useful data for modelling and physical interpretations in this key source. The MW data can help to distinguish between the jet/energetic and geometric/binary-BH scenarios; to clarify the relationship between the non-thermal random flaring events in the jet and the long-term cyclic outbursts; to understand MW correlations; to study acceleration/emission processes and the dynamics of the emitting regions.

Near-IR and optical light curves obtained with the collaboration of more than 30 ground-based observatories around the world, through the WEBT consortium[1] and the ENIGMA Network[2] during the campaign triggered by the first two spacecraft observations in 2005 are showed globally in Fig. 3. Moreover in Fig. 4 a detail of the better sampled light in *R*-band is showed.

The observing season spanning from Oct.2004 to May2005 has data from both the long-term monitoring and the intensive WEBT core campaign (5 days, Apr.10-14, 2005, around the first XMM-pointing date: April 12, 2005). In this period an intermediate and high brightness level at optical bands is observed. The brightness of OJ 287 increased of 2 mag in about 2.5 months and XMM-Newton observed the source during an optical flare: there was an increase of about 0.8mag in 8 days, a subsequent large drop of the flux of about 1.4mag in 13 days, and almost a 0.3mag brightness increase in less than 9 hours during the satellite observation time (Apr.12).

The observing season spanning from Oct.2005 to Apr.2006 has data from both the long-term monitoring and the intensive WEBT core campaign (about 20 days in Oct.-Nov. 2005, around the second XMM-pointing date: Nov.3-4, 2005). A quite amazing optical outburst showing a wiggling time-structure and persistence (duration more than 20 days) was discovered (Fig. 4 lower panel zoom). The second XMM-Newton observation was notably performed during this active phase.

4. X-ray behaviour

During the last 1994 optical outburst OJ 287 showed the synchrotron high-energy tail in the soft-X band, while in 1997 (during the brightness decline) it emitted a pure IC X-ray emission (Isobe et al. 2001). *Beppo*SAX also observed a relatively low X-ray flux F_X(2-10 keV) = (1.35 $\pm$ 0.15) $\times 10^{-12}$ erg cm^{-2} s^{-1}, corresponding again to pure IC emission (Massaro et al. 2003).

XMM-Newton EPIC (pn and MOS) instrument data provided us with crucial information on the high-energy spectral component (IC emission), while the radio-to-optical observations mapped the behaviour of the synchrotron emission component. Moreover, XMM-Newton OM instrument data can shed light on the high-frequency synchrotron tail, produced by the highest energy particles in the UV regime. Combined EPIC (pn, MOS1, MOS2 detectors) X-ray spectra of OJ 287 belonging to the first 2 observations in 2005 are showed in Fig. 5. The large frame and medium filter EPIC configuration was used, and intervals of high background radiation were filtered. Data were processed with XMM-

[1] http://www.to.astro.it/blazars/webt/
[2] http://www.lsw.uni-heidelberg.de/projects/enigma/

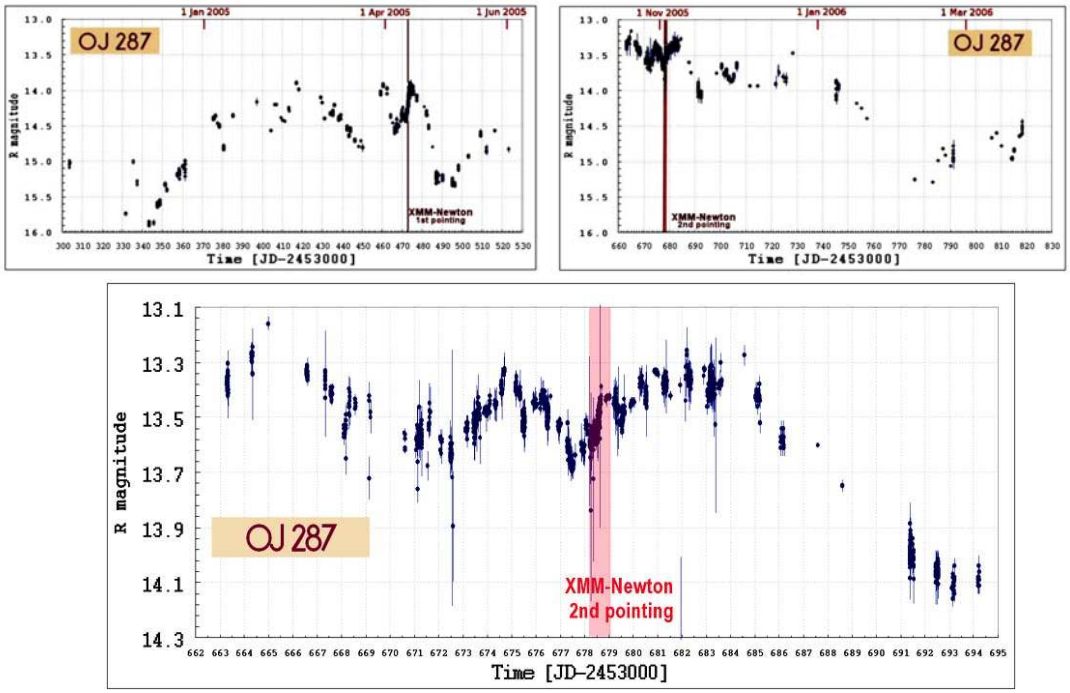

Fig. 4. The Oct.2004-Apr.2006 optical light curve (R-band) obtained during the extended coordinated campaign (XMM-Newton pointing dates are marked by the red lines). Data refers to the intensive WEBT coordinated campaign and long-term monitoring. XMM-Newton observed OJ 287 twice (Apr.12 and Nov.3-4, 2005), during 2 main optical flares (upper panels). In particular an enduring activity was observed in the optical regime during the second satellite pointing, $R_{max} = 13.2, 13.3$ (see the zoom in the bottom panel).

SAS v.6.5, and XSPEC. The Apr.12 spectrum can be preliminary described by a simple power-law plus galactic absorption, while the Nov.3-4 spectrum can be preliminary described by a broken power-law plus galactic absorption, with parameters values reported in the caption of Fig. 5. In summary different slopes and brightness, and possibly different components were detected in the X-ray spectrum of OJ 287.

5. Conclusions

This MW campaign devoted to OJ 287 (still on course) and organized within the EC Research Network ENIGMA can be considered quite a challenge. First of all it was the first campaign led, started with a XMM-Newton GO proposal and followed by requests, interactions, information exchanges and tuning with ground-based observatories. The subsequent stage was the collection, assembling, reduction and analysis of the X-ray and radio-optical datasets. In particular to be noted that heterogeneous optical data (produced usually from very different professional and amateur observatories) can be more difficult to be handled with respect to final radio data. Blazar MW campaigns are very useful for AGN science, promoting also international collaboration and public outreach aspects, but need of a quite large amount of time, of suitable manpower and experience, in order to be timely and well handled towards the final results.

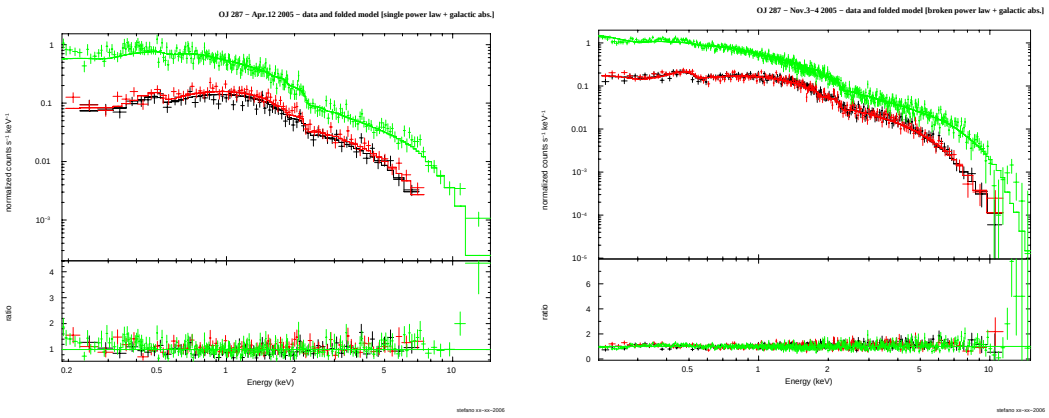

Fig. 5. XMM-Newton combined EPIC (pn, MO1 and MOS2 detectors) X-ray spectra of OJ 287 (z=0.306), belonging to the 2 observations performed on Apr.12, 2005 and Nov.3-4, 2005 (AO-4). In EPIC the large frame + medium filter configuration was used, and intervals of high background radiation were filtered. Data processed with XMM-SAS v.6.5, and XSPEC. *Left panel*: the Apr.12 spectrum can be described by a simple power-law + galactic absorption, $N_H = 3.09 \times 10^{20}$ cm^{-2}, $\Gamma = 1.628 \pm 0.023$, $\chi^2_r = 1.035$ $d.o.f. = 367$, $F_{2-10\mathrm{KeV}} = (2.47 \pm 0.8) \times 10^{-12}$ erg s^{-1} cm^{-2}. *Right panel*: the Nov.3-4 spectrum can be described by a broken power-law + galactic absorption, $N_H = 3.09 \times 10^{20}$ cm^{-2}, $\Gamma_1 = 2.65(-0.07/+0.12)$, $\Gamma_2 = 1.79 \pm 0.02$, $E_{br} = 0.69$ KeV, $\chi^2_r = 1.030$ $d.o.f. = 927$, $F_{2-10\mathrm{KeV}} = (1.82 \pm 0.07) \times 10^{-12}$ erg s^{-1} cm^{-2}.

References

Isobe N., Tashiro M., Sugiho M., & Makishima K. 2001, PASJ, 53, 79

Lehto H. J. & Valtonen M. J. 1996, ApJ, 460, 207

Massaro E., Giommi P., Perri M. et al. 2003, A&A, 399, 33

Nilsson K., Takalo L.O., Sillanpää A., & Ciprini S. 2006, ASP Conf. Ser. 350, 47

Sillanpää A., Takalo L. O., Pursimo T. et al. 1996, A&A, 305, L17

Shrader C. R., Hartman R. C., & Webb J. R. 1996, A&AS, 120, 599

Valtaoja E., Teräsranta H., Tornikoski M. et al. 2000, ApJ, 531, 744

Valtonen, M. J. et al. 2006a, ApJ, 646, 36

Valtonen, M. J. et al. 2006b, ApJ, 643, L9

Variability time scales from long term monitoring

T. Hovatta[1]*, M. Tornikoski[1], M. Lainela[2], E. Valtaoja[2,3], I. Torniainen[1], M.F. Aller[4], H.D. Aller[4]

[1]Metsähovi Radio Observatory
Metsähovintie 114, 02540 Kylmälä, Finland
[2]Tuorla Observatory
Väisäläntie 20, 21500 Piikkiö, Finland
[3]Dept. of Physical Sciences University of Turku, 20100 Turku, Finland
[4]Department of Astronomy, University of Michigan

October 27, 2006

Abstract

We have been studying the long term variability time scales of a large sample of Active Galactic Nuclei (AGNs), which have been monitored in the Metsähovi radio observatory at 22, 37 and 87 GHz. In the sample we have 80 sources from different AGN classes including BL lacertae objects (BLOs), highly polarized quasars (HPQs), low polarisation quasars (LPQs) and radio galaxies (GALs). In our study we used several frequency bands between 4.8 and 230 GHz. The lower frequency data at 4.8-14.5 GHz are from the University of Michigan Radio Observatory (UMRAO) and the higher frequency data at 90 and 230 GHz mostly from the SEST telescope. We used the structure function, discrete autocorrelation function and the Lomb-Scargle periodogram to derive the time scales. Motivation for using many methods, was to study the differences between the methods and the reliability of the results. Our results reveal that time scales shorten with increasing frequency. When considering the observational time scales we did not find significant differences between the AGN types. After redshift correcting the results, the time scales between the flares showed significant difference between the BLOs and the quasars. This means that the rate at which shocks are ejected into the jet is different for BLOs and quasars.

1 Introduction

Studying the long term variability of Active Galactic Nuclei (AGNs) can help us to better understand the observed phenomena in AGNs and also the differences between various AGN types. It is important to use many frequency bands to gain information about the evolution of variability at different frequencies. This way we can develop the shock models and better understand the physical processes in AGNs. The variability time scales tell us how often these sources are in a flaring state and how long these outbursts typically last. Depending on the method, we can find different time scales in the flux curves, for example the times between the flare peaks and the rise and decay times of flares.

There have been many studies of variability time scales for individual sources (eg. Villata et al. 2004, Ciaramella et al. 2004, Raiteri et al. 2003, Raiteri et al. 2001, Roy et al. 2000), but to our knowledge such a large sample of sources has never been studied over such a wide frequency range before. Hughes et al. (1992) used the structure function to study the characteristic time scales of a large sample of AGNs monitored in the University of Michigan Radio Observatory (UMRAO) at frequencies 4.8, 8 and 14.5 GHz. This study was done when approximately 15 to

*tho@kurp.hut.fi

20 years of monitoring data were available. Lainela & Valtaoja (1993) also used the structure function to study the time scales of 42 sources at 22 and 37 GHz. The sources had been monitored for 9 to 12 years at the Metsähovi Radio Observatory. One purpose of our study was to compare our results with results from Lainela & Valtaoja (1993) and find out how 13 years of more data affects the time scales.

In addition, we wanted to study the differences between the statistical methods and the results we obtain with them. Also the differences between various AGN types are studied. We have studied both the observational time scales and intrinsic time scales of these sources.

2 The sample and observations

The basis of this work is the monitoring data from Metsähovi Radio Observatory. We have been monitoring extragalactic radio sources at frequencies 22, 37 and 87 GHz for over 25 years (eg. Teräsranta et al. 2005). In addition we used lower frequency data from UMRAO, where some of the AGNs have been monitored for over 30 years. The higher frequency data at 90 and 230 GHz were mainly from Metsähovi and our monitoring campaign at the SEST telescope between 1987 and 2003 (Tornikoski et at. 1996, Tornikoski et al. 2006 in preparation). Data at higher frequencies were also collected from the literature (Steppe et al. 1988, 1992, 1993; Reuter et al., 1997)

Our sample consists of 80 sources from different AGN classes so that 24 of the sources are BL Lacertae objects (BLOs), 23 Highly Polarized Quasars (HPQs), 27 Low Polarization Quasars (LPQs), 5 Radio Galaxies (GALs) and one Empty Field source (EF). For 4 objects we had no information about the optical polarization and they are considered LPQs in this study. When we have studied the statistical differences of the various groups, only BLOs, HPQs and LPQs are considered.

3 Methods

We used three different methods to study the characteristic variability time scales of AGN: The Structure Function (SF), Discrete autocorrelation Function (DCF) and the Lomb-Scargle periodogram (LS-periodogram). The logarithmic SF focuses more on the finer structural changes of the flux curve and gives a time scale related to the rise and decay times of the flares. The Lomb-Scargle periodogram is used to study the periodicities and from it we get a time scale between the flares. The DCF also concentrates more on the time scales between the outbursts but sees the finer structure as well. Therefore it combines some properties of the two other methods.

4 Results and discussion

We got 411 structure functions, discrete correlation functions and Lomb-Scargle periodograms. On average we had data at 5 frequencies for each source. The number of time scales we got with each method varied between the methods. From the structure functions we got 447 time scales, from the DCF 1020 and from the LS-periodogram 780. The lower number of time scales from the SF analysis is caused by the time scales being different from those in the other two methods. In DCF and LS-periodogram analysis we obtained over 10 time scales for some sources whereas for others we could not find any time scales. For those sources we determined a lower limit time scale of T/2, where T is the total observing period.

We calculated the averages of the most significant time scales for all frequencies by using all different methods. The averages are listed in Table 1. For the DCF and LS-periodogram we have also listed the averages without the lower limit estimates. These are shown in the parenthesis. We can see that the SF gives shorter time scales than the other two methods. In the SF there is

Table 1: Averages of the most significant time scales at all methods and frequencies. The time scales are in years and in parenthesis are the averages without the lower limit estimates

Freq (GHz)	SF	DCF	Periodogram
4.8	5.2	6.6 (5.1)	8.7 (7.5)
8	5.6	9.4 (7.1)	9.7 (9.0)
14.5	4.3	8.1 (6.6)	8.5 (8.0)
22	4.1	5.6 (4.4)	6.6 (5.5)
37	2.6	5.1 (4.1)	7.0 (6.2)
90	2.0	3.8 (3.5)	4.9 (3.7)

also a large difference between the averages of 22 GHz and 37 GHz. This is because at 22 GHz there is one source with a lower limit estimate time scale of 22 years, and it affects the average value. The median values in the case of SF are closer to each other and approximately 2 years for both of the frequencies.

The averages also shorten with increasing frequency. It may be due to the flares being superposed at lower frequencies and individual peaks are not as clearly distinguishable as at higher frequencies. Sometimes we can see shorter time scales because of the same effect, when the methods take into account the smaller variations at shorter time scales because there are no big outbursts present in the flux curve.

We ran a set of Kruskal-Wallis one way analysis of variance to test if there are differences between the frequency bands or the source classes. For all the methods, the frequency bands formed different subgroups and in general the higher frequency bands from 22 GHz upwards differed from the lower ones.

The same analysis for the source classes did not reveal any certain type of objects to be different from others. We got significant differences at some of the well monitored frequency bands, but none of the classes differed from others at all frequency bands or methods.

4.1 Re-analyzed structure functions

One purpose of our study was to compare the new structure function time scales with the earlier analysis from Lainela & Valtaoja (1993). Our samples had 40 sources in common and for these we could compare the results at 22 and 37 GHz. One difference is that in our analysis we did not find any significant differences between the source classes whereas the old analysis showed a significant difference between the HPQs and LPQs. The average time scales of our analysis were also slightly longer. This was partly due to some sources having only a lower limit time scale. In those cases the time scale of our analysis was much longer because of the longer observing period.

In general the number of such lower limit estimates had decreased from 32 to 10 in the new analysis. This is not surprising as we expect to see the characteristic behaviour of the AGNs when the monitoring has lasted longer. This result also tells us that there are still some sources for which we, after 20 years of monitoring, cannot determine the characteristic time scales. Certainly long term monitoring is needed to understand all the features of AGNs.

4.2 Intrinsic time scales

We have also studied the intrinsic time scales of these sources. We corrected the most significant time scales of all methods for the redshift and calculated the averages. We also ran the Kruskal-Wallis analysis to see if there is some difference between the source classes when intrinsic time scales are considered. In the SF and DCF analysis we got quite similar results as before and found no significant differences in most of the frequency bands. None of the source classes was different at all frequency bands. In the LS-periodogram analysis we could, however, detect a

Table 2: Average time scales from periodogram analysis. Both the observational and intrinsic time scales are listed

Freq (GHz)	BLO	BLO intrinsic	HPQ	HPQ intrinsic	LPQ	LPQ intrinsic
4.8	9.58	7.08	7.34	4.02	9.15	4.49
8	9.38	6.84	9.52	5.07	9.76	4.94
14.5	7.83	6.13	8.59	4.73	8.87	4.26
22	6.50	5.02	6.39	3.36	6.87	3.18
37	7.03	5.50	6.74	3.57	7.28	3.55
90	4.90	2.89	5.10	2.94	4.58	2.62

significant difference between the BLOs and the quasars at almost all frequency bands. The observational and intrinsic time scale averages from the periodogram analysis at different source classes are listed in table 2.

A clear difference can be seen between BLOs and quasars in the intrinsic time scales. The time scales of BLOs are about 2 years longer than those of quasars. There is no clear difference between the classes if we consider the observational time scales. The difference in intrinsic time scales was significant ($> 95\%$) at 4.8, 22 and 37 GHz. At 8 and 14.5 GHz the chance for BLOs and quasars being from the same populations was about 10%. At 90 GHz the sources are undersampled and we cannot make any concrete statistical conclusions from the analysis.

We believe that the reason why we could detect these differences only in the periodogram time scales is because it is the method which gives the time scale closest to the one between the flares. Physically this reveals the times between the shocks in the jet, and these should not be affected by the Doppler boosting effects. The SF and DCF also consider the rise and decay times from flares and these are affected by the Doppler boosting, and therefore we cannot see differences between the classes. This also means that the rate at which shocks are ejected into the jet is different for BLOs and quasars.

5 Conclusions

Our results revealed that we can find smaller flux variations in these sources in short time scales but the large outbursts occur quite rarely, on average in every 7 years. Therefore the long term monitoring is essential to understand the true behaviour of AGN. We found out that there is a significant difference between the BLOs and quasars when the intrinsic time scales are considered so that the time scales from BLOs are approximately 2 years longer than time scales of quasars. There were no differences between the source classes if only the observational time scales are considered.

6 Future

We are planning to study the correlations of time scales between the luminosities of the sources and also between the different jet parameters, the Doppler boosting factor, the Lorentz factor and the viewing angle. These will be taken from the paper by Lähteenmäki et al. (1999). Later we will also redo the calculations of the parameters with the more data now available. We will also study the individual flares of this large sample in more detail. This is already being done for the BLOs in a forthcoming paper by Nieppola et al. (2006, in preparation), where also the time scales of BLOs are studied in more detail.

Acknowledgements. UMRAO is supported in part by a series of grants from the NSF and by funds from the University of Michigan Department of Astronomy.

7 References

Ciaramella, A., Bongardo, C., Aller, H.D. et al.: 2004, *A&A*, **419**, 485
Hughes, P., Aller, H., & Aller, M.: 1992, *ApJ*, **396**, 469
Lainela, M. & Valtaoja, E.: 1993, *ApJ*, **416**, 485
Lähteenmäki, A., Valtaoja, E. & Wiik, K.: 1999, *ApJ*, **511**, 112
Raiteri, C., Villata, M., Aller, H.D. et al.: 2001, *A&A*, **377**, 396
Raiteri, C., Villata, M., Tosti, G. et al: 2003, *A&A*, **402**, 151
Reuter, H.-P., Kramer, C., Sievers, A. et al.: 1997, it A&AS, **122**, 271
Roy, M., Papadakis, I.E., Ramon-Coln, E. et al.: 2000, *ApJ*, **545**, 758
Steppe, H., Liechti, S., Mauersberger, R. et al.: 1992, it A&AS, **96**, 441
Steppe, H., Paubert, G., Sievers, A. et al.: 1993, it A&AS, **102**, 611
Steppe, H., Salter, C.J., Chini, R. et al.: 1988, it A&AS, **71**, 317
Teräsranta, H., Wiren, S., Koivisto, P., Saarinen, V. & Hovatta, T.: 2005, *A&A*, **440**, 409
Tornikoski, M., Valtaoja, E., Teräsranta, H. et al.: 1996, it A&AS, **116**, 157
Villata, M., Raiteri, C.M., Aller, H.D. et al: 2004, *A&A*, **424**, 497

Progress in Our Understanding of Blazars[1]

Alan P. Marscher[2]
Institute for Astrophysical Research, Boston University
marscher@bu.edu; website: http://www.bu.edu/blazars

[2]External advisor to the ENIGMA network

Abstract

I bid adieu to the ENIGMA collaboration by reflecting briefly on what the community has figured out about blazars and what puzzles remain. We have triumphed over a puzzling array of observations to develop a basic phenomenological picture that probably gets at least some of the physics right. But there remain scandals, areas where progress has been limited or the data seem to be contradictory to prevailing models.

Introduction

Sometimes when our data seem to defy all our attempts to explain them, we start to question whether we are certain of anything at all about blazars. It is therefore good for the soul to step back on occasion and consider what parts of our picture of blazars we can draw with confidence and compare this with what we knew a few decades ago before the current golden age of sensitive telescopes observing across the electromagnetic spectrum. Then we must return to reality and realize that there are still many aspects of these delightfully capricious objects that we do not understand well at all. This is my intention here, although I will avoid being comprehensive in order to maintain brevity and to allow me to discuss mostly my own viewpoint.

The General Picture

The fact that we have made enormous progress in our description of blazars is evidence by our ability to draw a cartoon against with which almost no one working in the field would find fault. Figure 1 displays my version, drawn with SuperMongo. We know that blazars are active galactic nuclei (AGN) with highly relativistically flowing plasma jets pointing almost right at us. We have strong evidence for an accretion disk surrounding a supermassive black hole at the center with some hot electrons above the disk (a “corona”) that scatter photons up to X-rays, and dense clouds that produce broad emission lines in the disk and winds within the inner parsec or so. The radio-emitting section of the jet is turbulent, and shocks or other disturbances passing through it create the appearance of bright knots that appear to move outward at superluminal speeds. The jet relativistically beams synchrotron and inverse Compton radiation from radio to gamma-ray frequencies.

Much of this emission occurs in such compact regions and with strong blueshifting that blazars are extreme variables at every frequency at which we can observe them.

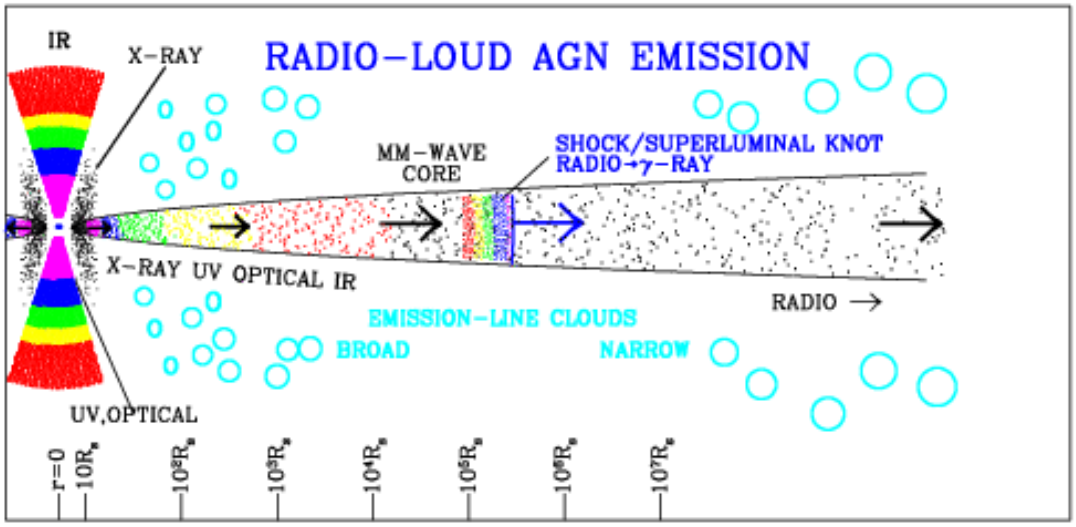

Figure 1. The author's cartoon of the emission components of a radio-loud active galactic nucleus. The length scale is logarithmic, as indicated by the scale at the bottom.

How certain are we of this description of a blazar, which owes its origin to Blandford & Rees (1978) and Blandford & Königl (1979)? I think very certain: all of us would be astonished if any part of the previous paragraph were demonstrated to be invalid. But this is only a rough sketch. There are numerous details and even some general characteristics about which we have yet to confirm our suspicions. I outline these in the "Scandals" section. Nevertheless, the standard relativistic jet model agrees very well with the basic observations that we have gathered.

Lorentz Factors of the Jet Flow

One of the basic parameters that governs the emission and apparent motions that we see in blazars is the bulk Lorentz factor of the jet. We can obtain a lower limit to this from the apparent superluminal motion of bright knots that we see on VLBI images. Although it is theoretically possible for the knots to be moving much faster than the ambient jet flow, we don't expect this to be the case, since the shocks are rarely very strong (e.g., Hughes, Aller, & Aller 1985,1989). We can estimate the actual Lorentz factor rather than a limit by obtaining the value of the Doppler factor needed to shorten the timescale of variability to an acceptable value. Valtaoja & Lähteenmäki (2003) have done this for a number of blazars under the assumption that the brightness temperature must obey the 10^{12} K limit. Kellermann et al. (2004) have modified this by combining the apparent speed with the brightness temperature corresponding to the emitting region maintaining equipartitition between the energy densities of the electrons and the magnetic field, as one might expect for a turbulent plasma. Jorstad et al. (2005) improve on these methods by measuring the size of a knot along with its apparent speed and timescale of decline in flux density.

The results of these methods are separate values of the Doppler factor, Lorentz factor, and angle of velocity vector to the line of sight of individual knots in a number of blazars. This leads to an upward revision of the bulk Lorentz factor of some well known blazars. For example, in 3C 279 the bulk Lorentz factor is as high as ~25 and the Doppler factor ranges up to ~50, depending on the angle that the somewhat jittery jet makes to the line of sight. To reward this deduction, made from data obtained between 1998 and 2001, during the period 2001 to 2004 3C 279 displayed superluminal motion as high as ~ 20*c*. We can now understand why this quasar is among the most dramatic blazars. The changes that we observe in apparent speed in 3C 279 may be due solely to variations in the direction of jet by about ±2°.

The fastest apparent speed that we can attest to with confidence (i.e., measured for a bright knot identified across epochs by its direction of linear polarization) is 45*c*, (in the extreme blazar PKS 1510-089), which allows a Doppler factor of 90 when the jet points directly at us. This is consistent with the highest variability Doppler factors reported thus far.

We can ask the question of whether the statistics of the radio-loud AGN population makes sense given the Doppler factors that we observe in the most extreme objects. We know that relativistic beaming causes a strong selection effect in flux-limited radio surveys: there is a bias toward jets with high Lorentz factors that point almost directly along line-of-sight. The population simulation of Lister & Marscher (1997) reproduces the observed apparent-motion & redshift distribution if:
1. The radio-galaxy luminosity function measured at low redshift z is valid at higher z
2. The Lorentz factor (Γ) distribution is a power law, $N(\Gamma) \propto \Gamma^{-a}$, a = 1.5-1.75, with a high-Γ cutoff of 45.
With these parameters, we find that 12-17% of jets in the parent population have Γ = 10-45, 5-7% have Γ = 20-45, 2-3% have Γ = 30-45, 0.5-0.9% have Γ = 40-45. That is, roughly 85% of all jets have Lorentz factors below 10. I do not think that the statistics can accommodate jet models featuring an ultra-fast ($\Gamma > 10$) spine and a slower sheath in all cases (e.g., Sol, Pelletier, & Asséo 1989; Punsley 1996; McKinney 2006). In the author's opinion, the data are more consistent with a spine that has a modest Lorentz factor in most cases, perhaps surrounding by a sheath that flows at mildly relativistic speeds.

Opening Angles of Jets

Since we see jets projected onto the sky plane, we would expect that blazars would all display very wide opening angles. The opening angles typically seen in the nearly side-on jets of radio galaxies typically range from about 1°-4°. Even if we take the lower value in this range, we would expect the opening angle to be proportional to apparent speed. For example, the opening angle of the jet in 3C 279 should be of order 20°. Instead, its jet is rather thin. Jorstad et al. (2005) have uncovered the reason for this: the intrinsic opening angle of a jet is inversely proportional to its Lorentz factor.

This dependence agrees with models in which jets are focused as they accelerate over an extended region (gas dynamics: Marscher 1980; magnetohydrodynamics: Vlahakis & Königl 2004). We will return to this when discussing models for the core.

Shocks and Turbulence

The favorite current model for the superluminal knots is that they represent internal shocks propagating away from the central engine. Marscher and Gear (1985) developed a model for variability of the continuum spectrum of blazars based on this idea. If the electrons are accelerated at the shock front and then lose energy as they advect away from the front, the emission region is frequency stratified, with the highest frequencies of synchrotron radiation produced in a thin layer behind the shock front and lower frequencies spread over a larger volume. This steepens the synchrotron spectrum of the synchrotron spectrum by 0.5, from a slope of $-(s-1)/2$ to $-s/2$, where $-s$ is the slope of the electron energy distribution. As the shock moves down the jet into regions of weaker magnetic field – and therefore less severe radiative losses – and lower density, the self-absorption spectral peak decreases while the flux density at the peak changes slowly. Eventually, the shocked region expands adiabatically and the peak flux density declines monotonically. This spectral evolution matches fairly well the observed behavior of blazars (e.g, Valtaoja, Lähteenmäki, & Teräsranta 1992; Türler et al. 1999).

Shocks also provide an explanation for the polarization in many blazars. In general, the polarization in the cores is of order a few percent even at high frequencies (Marscher et al. 2002), indicating a mostly chaotic magnetic field configuration. Since a shock front amplifies the component of the field that lies parallel to the front, the field is partially ordered behind the shock front and the polarization electric vector tends to be transverse to the front. This matches the observed polarization in many blazars (Hughes, Aller, & Aller 1985, 1989). The initial supposition that the shocks are transverse to the jet axis has given way to oblique shocks, as seen in 3D gas dynamical simulations (Hughes 2005). (The mistaken impression that so many fields are transverse to the axis occurs if one forgets to take into account relativistic aberration.) In addition, many quasars have polarizations essentially parallel to the axis. This can be accomplished through velocity shear, i.e., cross-jet gradients in flow Lorentz factor (see Fig. 2 and Laing 1980). The shocks needed to explain variability are usually quite weak, with compression by a factor of ~1.2, which in many blazars is not enough to overcome the ordered component of the field parallel to the axis. Weak shocks make sense theoretically, since relative motions need to be supersonic to get shock waves. Application of the formula for relativistic addition of velocities demonstrates that strong shocks are difficult for a high-Γ flow with a relativistic equation of state to form.

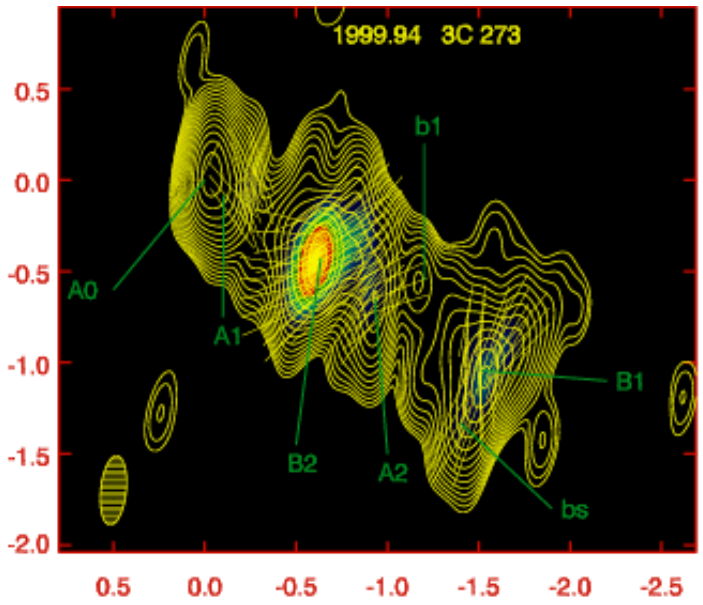

Figure 2. VLBA image of the quasar 3C 273. The polarization electric vector is nearly perpendicular to the jet axis, indicating that the ordered component of the magnetic field is roughly parallel to the axis. This is probably the result of velocity shear. Indeed, knots on the northern side have bulk Lorentz factors ~ 8, while those on the southern side have values ~ 14.

The Core

One of the least well understood aspects of radio-loud AGN is the nature of the core at millimeter wavelengths. The cm-wave core is well explained as the point in the jet where the optical depth to synchrotron radiation is roughly unity, although the polarization suggests that in some cases it might be the first standing shock system downstream of this point. (Daly & Marscher 1988; Jorstad et al. 2005). But is is less clear why the jet emission at short millimeter wavelengths, where the spectrum indicates it is optically thin, starts many thousands of Schwarzschild radii from the central black hole.

A leading possibility is that the mm-wave core is the end of the zone of acceleration of the flow (Marscher 1980). If the jet points toward us, this is where the emission coefficient – that is, the combination of $N_o B^{1+\alpha}\delta^{2+\alpha}$, where the electron energy distribution is $N_o E^{-(2\alpha+1)}$, B is the magnetic field, and δ is the Doppler beaming factor – reaches its highest value. In non-blazars, such as Cygnus A, beaming is not as important, so the core would lie closer to the central engine, probably at the innermost region of particle acceleration.

Jet acceleration over such an extended region is a feature of the magnetohydrodynamic jet launching model of Vlahakis & Königl (2004). While these models are still under development, they have certain features in common. For example, the flow Lorentz factor Γ decreases away from jet axis, which could lead to the velocity shear and turbulence that we infer to occur downstream of the jet acceleration zone (see above). In order for the jet to attain a high value of Γ, the magnetic energy density at the base must exceed ~ $2\Gamma\rho c^2$, where ρ is the mass density. While this seems at first to be difficult to imagine, if the

twisting magnetic field that focuses the jet originates in the ergosphere of a spinning black hole, it is difficult to understand how *any* particles can get into the jet, which should be almost completely Poynting flux dominated.

The magnetic collimation models (Meier, Koide, & Uchida 2000) predict a tightly wound helical magnetic field geometry within the jet acceleration zone. Any synchrotron radiation from this region should have a polarization direction that is either parallel or perpendicular to the axis (Lyutikov, Pariev, & Gabuzda 2005). Multiwaveband polarization observations might have seen this at 1 mm (Jorstad et al.2007).

Connection between the Jet and the Central Engine

The author's group has studied time variations in the X-ray emission – mostly from the central engine – and the jet of two blazar-like radio galaxies. As published in Marscher et al. (2002), in the FR1 source 3C 120 the appearance of bright superluminal knots follows spectrally hard dips in the X-ray flux. Our continued observations since early 2002 confirm the trend. This strongly suggests a connection between X-rays from the "corona" above the accretion disk and activity in the jet. This is similar to the behavior of microquasars, but not as dramatic in that the X-ray state does not exhibit abrupt changes. It is possible that such changes do occur in AGN but on time scales much longer than we have been observing their X-ray and radio emission.

The FR2 radio galaxy 3C 111 appears to behave in the same manner as 3C 120, but thus far we have observed only three pairs of X-ray dips and superluminal ejections, so we need more data to verify this.

In the case of 3C 120, we can say that the 3mm core must lie at least 0.4 pc from the black hole to produce the observed X-ray dip/superluminal ejection delay of ~ 60 days. This again points to acceleration of the jet over a large distance from the central engine.

Changes in Jet Direction and OJ 287

An interesting question is the stability of the direction of a jet. Does it wiggle sporadically or perhaps precess systematically, as one might expect in the case of a binary black hole? Is the apparent swing in direction of the jet accompanied by changes in the variability properties expected if the Doppler factor varies? In fact, the direction of jets on the sky does vary, and some have interpreted the swings in terms of precession. My own, tentative conclusion is that the changes are not sufficiently systematic to be caused by precession. Because of projection effects, the actual, i.e., 3D, change does not need to be more than a few degrees, but this is still quite a substantial shift in momentum. The X-ray variability states of 3C 279 and PKS 1510-089 appear to be related to the projected directions of their jets, but more data are required to corroborate this tendency.

Since a long-term periodicity of roughly 12 years has been claimed in the BL Lac object OJ287 (Sillanpää 1988), we should ask whether there is any evidence for a change in the direction of the jet that could cause a panchromatic outburst. Figure 3 provides some

snapshots of the jet at 43 GHz across a time span of 9.5 years. This suggests the possibility of precession, although the period would need to be much longer than the claimed 12-year period between major outbursts. We cannot, however, rule out a period twice as long, with outbursts during each half-cycle.

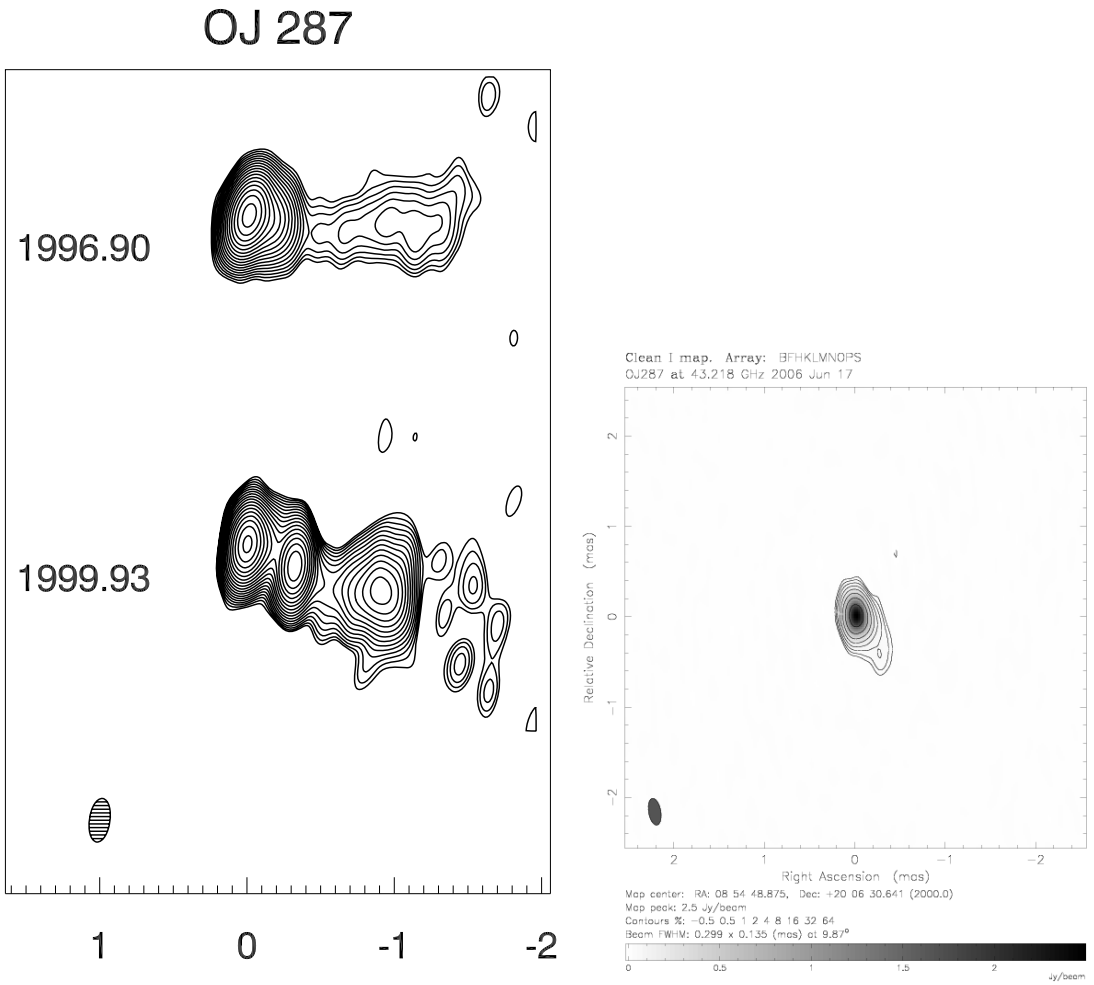

Figure 3. VLBA images at 43 GHz of OJ287 at three epochs over a 9.5 year time interval. The change in the apparent direction of the jet has been dramatic.

Scandals

I have summarized some notable progress that we have made in our attempts to understand the enigmatic beasts we call blazars. There remain, however, some rather embarrassing gaps in our knowledge and in our techniques at exploring the physical nature of these objects. I list here many of the shortcomings that I see, in no particular order.

- We are quite unsure of what the mm-wave core is despite its prominence.

- TeV BL Lac objects exhibit slow apparent speeds and weak radio variability, yet need high Doppler factors.
- The shock model for flares, more than 20 years old, provides no description of the rising flux. (The author disowns the "Compton stage" – light-travel effects make this phase more complex than the treatment found in Marscher & Gear 1985.)
- Flare profiles are sharply peaked, yet in nearly all models they are rounded or flat.
- Particle acceleration models are only partially developed. How can most particles be relativistic? How can we get energies ~10-100 TeV?
- Some blazars are extremely strong scintillators at low frequencies, which implies extreme compactness, as parametrized by the minimum brightness temperature. Can the Doppler factor be as high as ~200? Population statistics suggest that this is not the case.
- Models for very high γ-ray luminosities involve inverse Compton scattering of photons external to jet. However, mm-wave flares often precede γ-ray flares, which implies that the latter are produced outside the broad emission-line region.
- We have no complete samples of quasars**.** Samples are always dominated by selection effects.
- Nature keeps jets together that 3D hydrodynamical simulations destroy.
- Single-zone models are widely applied to rapid variations, while we know that we need to include frequency stratification and light-travel effects.
- There is no model for what must be a rather abrupt transition from toroidal to turbulent magnetic field in the jet.
- Jets contain mostly relativistic plasmas; we are ignorant of the physics of such plasmas.
- Jets change direction, usually non-periodically; we do not know why.
- Core-sheath models of jets give us extra free parameters but have not yet been tested against existing statistics.
- The extreme blazars 0716+714 refuses to give us its redshift, so we do not know exactly how extreme it is.

Conclusions

I think that we should be encouraged by progress in our field. However, we need to keep in mind when we construct crude models that the details may eventually destroy them. We will have a great opportunity to continue testing our ideas when GLAST and AGILE are recording well-sampled light curves. And of course there is the predicted big OJ 287 blast in late September 2006 that should either vindicate the binary black hole model or send its proponents back to the drawing board. We should not despair if the latter occurs: it is the capricious behavior of blazars that we find so tantalizingly attractive!

Acknowledgments

The opinions expressed here are based on research by the Blazar Group at Boston University, which is supported in part by National Science Foundation grant AST-0406865 and a number of NASA grants, most recently NNG05GM33G and NNG05GO46G. The group includes Dr. S. Jorstad, whose collaborative work with the

author is liberally distributed throughout this paper. The VLBA is an instrument of the National Science Foundation operated by the National Radio Astronomy Observatory under cooperative agreement by Associated Universities Inc.

References

Blandford, R. D., & Königl, A. 1979, ApJ, 232, 34
Blandford, R. D., & Rees, M. J. 1978, in Pittsburgh Conference on BL Lac Objects, ed. A. M. Wolfe (U. Pittsburgh Press),
Daly, R. A., & Marscher, A. P. 1988, ApJ, 334, 539
Hughes, P. A. 2005, ApJ, 621, 635
Hughes, P. A., Aller, H. D., & Aller, M. F. 1985, ApJ, 298, 301
Hughes, P. A., Aller, H. D., & Aller, M. F. 1989, ApJ, 341, 54
Jorstad, S. G., et al. 2005, AJ, 130, 1418
Jorstad, S. G., et al. 2007, ApJ, submitted
Kellermann, K. I., et al. 2004, ApJ, 609, 539
Laing, R. A. 1980, MNRAS, 193, 439
Lister, M. L., & Marscher, A. P. 1997, ApJ, 476, 572
Lyutikov, M., Pariev, V. I., & Gabuzda, D. C. 2005, MNRAS, 360, 869
Marscher, A. P. 1980, ApJ, 235, 386
Marscher, A. P., et al. 2002, Nature, 417, 625
Marscher, A. P., & Gear, W. K. 1985, ApJ, 298, 114
Marscher, A. P., Jorstad, S. G., Mattox, J. R., & Wehrle, A. E. 2002, ApJ, 577, 85
McKinney, J. A. 2006, ApJ, in press
Meier, D. L., Koide, S., & Uchida,Y. 2000, Science, 291, 84
Punsley, B. 1996, ApJ, 473, 178
Sillanpää, A., et al. 1988, ApJ, 325, 628
Sol, H., Pelletier, G., & Asséo, E. 1989, MNRAS, 237, 411
Türler M., et al., 1999, A&AS, 134, 89
Valtaoja, E., & Lähteenmäki, A. 2003, ApJ, 590, 95
Valtaoja, E., Lähteenmäki, A., & Teräsranta, H. 1992, A&AS, 95, 73
Vlahakis, N., & Königl, A. 2004, ApJ, 605, 656

The research of BL Lacertae objects in Metsähovi Radio Observatory

E. Nieppola[1,2]*, M. Tornikoski[1], A. Lähteenmäki[1], E. Valtaoja[2,3]

[1]Metsähovi Radio Observatory
Metsähovintie 114, 02540 Kylmälä, Finland
[2]Tuorla Observatory
Väisäläntie 20, 21500 Piikkiö, Finland
[3]Dept. of Physical Sciences
University of Turku, 20100 Turku, Finland

October 27, 2006

Abstract

We present the Metsähovi Radio Observatory research related to BL Lacertae objects during the ENIGMA era. The Metsähovi BLO sample consists of 398 objects. For most of them, we have determined the spectral energy distribution (SED) using archival multi-frequency data. We fitted a parabolic function to the synchrotron component of the SEDs and calculated the synchrotron peak frequencies, ν_{peak}, of the sample sources. When we studied the correlations of ν_{peak} and the source luminosities on several wavelengths, we found that the peak luminosity does not depend on ν_{peak}, contrary to the blazar sequence scenario. We also give a summary of the BLO observing project at Metsähovi and the impending BLO data publication, and close with some plans for the future.

1 Introduction

BL Lacertae objects (BLOs, BL Lacs) are AGNs which have their jets closely aligned towards us. This makes their characteristics seem extreme; typically they exhibit strong and rapid variability in several frequency bands, high optical polarization and near-featureless spectra (Stein et al. 1976; Kollgaard 1994; Jannuzi et al. 1994). BLOs can be further classified according to two different schemes (Giommi et al. 1995; Padovani & Giommi 1995; Sambruna et al. 1996). One is based on the frequency band of the survey in which they were discovered. Then they are either radio-selected (RBLs) or X-ray-selected (XBLs). The other scheme has a more physical basis. It classifies a source according to the peak frequency of the synchrotron emission, ν_{peak}, in its spectral energy distribution (SED); if it is at low frequencies we have low-energy BL Lacs (LBLs), and in the other end we have high-energy BL Lacs (HBLs). Objects which are in between the classifications (in either scheme) are referred to as intermediate BL Lacs (IBLs) (Laurent-Muehleisen et al. 1999; Bondi et al. 2001).

The reason behind such differences in peak frequencies has remained obscure. Fossati et al. (1998) linked the source luminosity and ν_{peak} in the well-known blazar sequence scenario, which states that the lower the peak frequency, the higher the luminosity. It has since been brought into question by the possible discovery of high-luminosity HBLs (Giommi et al. 2005) and low-luminosity LBLs (Padovani et al. 2003).

In this paper we describe the BLO-related activities of the Metsähovi team during the ENIGMA era. They can be roughly divided into two parts; work related to the spectral energy

*eni@kurp.hut.fi

distributions and classification of BLOs (Nieppola et al. 2006a), and the Metsähovi BLO observing project and its results (Nieppola et al. 2006b). We give an overview of both, and finish with a look into the future.

2 Determining the SEDs

2.1 Collecting and fitting the data

The classification schemes of BLOs have been typically tested with moderate-sized samples, which usually consist of only relatively bright sources. The Metsähovi BLO sample contains almost 400 objects, most of which are quite faint. To find out the subgroup of each source, we set out to plot their spectral energy distributions.

In order to determine the SED of as many objects as possible, we searched for a large amount of multi-frequency archival data from databases and the literature. Naturally the starting point was the Metsähovi 37 GHz BLO observing project data (see Section 3), helping to narrow the wide gap between the low radio and optical wavelengths. Our main data source was the CATS[1] database (Verkhodanov et al. 1997), maintained by the Special Astrophysical Observatory of Russia. The synchrotron components of the SEDs were fitted with a parabolic function $y = Ax^2 + Bx + C$ (Nieppola et al. 2006a). The fitting was successful for 304 sources.

The question of whether or not to include the X-ray datapoints to the synchrotron component was problematic. In LBLs, the X-ray flux is dominated by the inverse Compton radiation, whereas in HBLs it is synchrotron radiation. Typically there are very few X-ray datapoints available for these sources, which means we have no information about the shape of the X-ray spectrum. Thus, we could only rely on a visual estimation of the most probable shape of the synchrotron component. Some examples of the SEDs are shown in Fig. 1.

For each fit we determined the peak frequency and divided the sources to LBLs, IBLs and HBLs accordingly. We chose the limits as follows: for LBLs $\log \nu_{peak} < 14.5$, for IBLs $14.5 < \log \nu_{peak} < 16.5$ and for HBLs $\log \nu_{peak} > 16.5$. The sample divided into the three classes quite evenly: there were 98 LBLs, 96 IBLs and 110 HBLs. The distribution of the peak frequencies is shown in Fig. 2

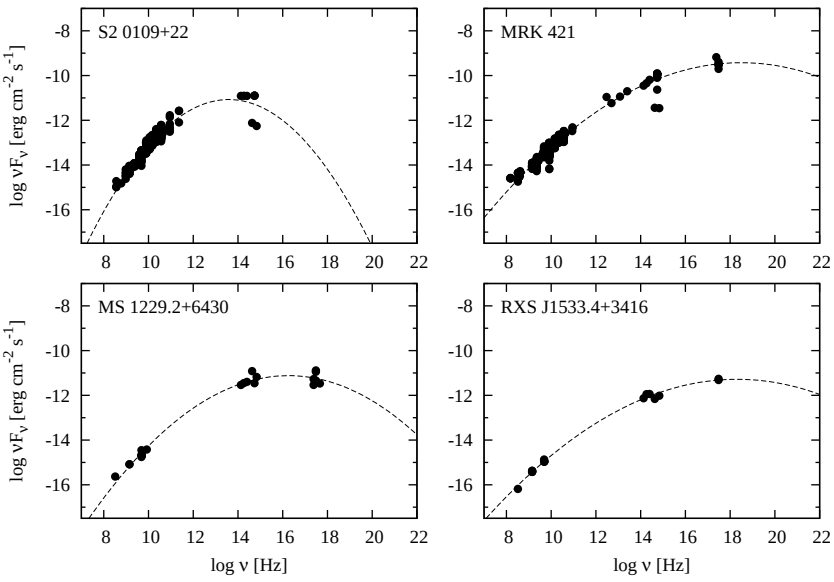

Figure 1: Some examples of the SEDs. Only datapoints used in the fit are shown.

[1] http://cats.sao.ru

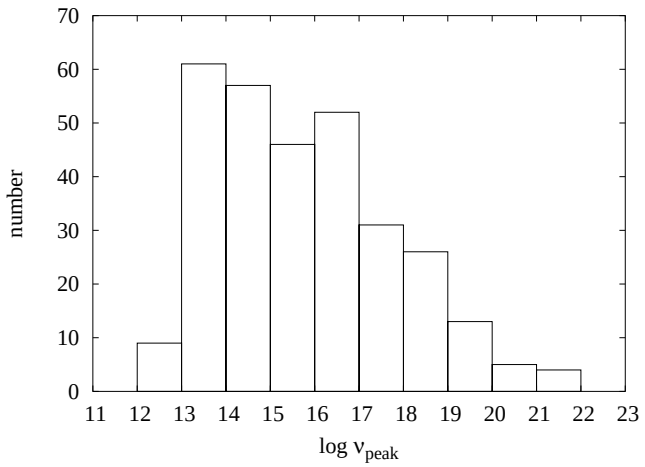

Figure 2: The distribution of the synchrotron peak frequencies in the Metsähovi sample.

Table 1: Division of observational BL Lac classes to physical ones.

	LBL	IBL	HBL
RBL	84 %	10 %	6 %
IBL	22 %	36 %	42 %
XBL	21 %	25 %	54 %

2.2 Results

Fig. 2 illustrates how the BLO population is continuous, with no significant clustering in either end of the peak frequency range. The highest peak frequencies are very high indeed, over $\log \nu_{peak} > 20$. This is partly an effect caused by the fit function. When the X-ray datapoints are included in the synchrotron component, the parabolic function tends to peak well after the X-ray domain. In reality, we would expect it to decline more steeply. Examples of this effect can be seen in Fig. 1, in the fits of Mrk 421 and RXS J1533.4+3416.

Although the highest peaks can be exaggerated, they still are quite exceptional sources. Even the most extreme HBLs are usually thought to peak in the X-ray region, but there has been some speculation about the existence of objects peaking in the MeV-region (Ghisellini 1999; Giommi et al. 2001). At least some of these could be considered as candidates for such sources.

Table 1 presents how the observational classification corresponds to the physical one. We see that a large majority of RBLs are LBLs, only 6% are in fact HBLs. XBLs, however, are quite frequently LBLs or IBLs, and only half of them are pure HBLs. This means that X-ray surveys are more likely to find LBLs than radio surveys are to find HBLs.

To test the blazar sequence scenario, we calculated the luminosities in many frequency bands and checked their dependence of ν_{peak}. While LBLs are significantly more luminous at radio wavelengths than HBLs, there seems to be no such correlation between ν_{peak} and peak luminosity L_{peak} (Fig. 3). We considered the effect that the exaggerated peak frequencies mentioned before could have on this correlation. We artificially lowered the values of ν_{peak} and peak luminosity to see if this would change the appearance of Fig. 3. While the farthest datapoints move slightly towards lower left, it would require a dramatic alteration of their L_{peak} to change the fundamental result.

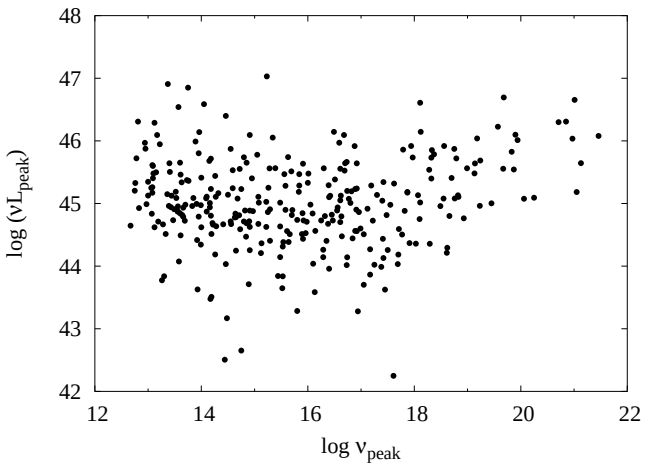

Figure 3: The peak luminosity, L_{peak}, plotted against the peak frequency, ν_{peak}.

3 Metsähovi 37 GHz BLO observing project

3.1 Observations

The Metsähovi radio telescope is a radome-enclosed antenna with a diameter of 13.7 metres. It is situated 60 m above sea level at the latitude of 60^o13'05"N. Metsähovi Observatory has been observing AGNs for nearly 30 years. This long term monitoring list includes also many of the best-known BL Lacs, like OJ 287, S5 0716+714, and BL Lac itself. In 2001, we started observing an extended source list of 398 BLOs. This sample includes all BLOs known at the time which can be observed from our northern location. The basis of our source list is the 9th edition of the Veron-Cetty & Veron BL Lac catalogue (Veron-Cetty & Veron 2000). In addition, 17 sources are taken from literature. Details about the observing system and data reduction at Metsähovi can be found in Teräsranta et al. 1998. The detection limit in Metsähovi is 0.2-0.5 Jy, depending on the weather.

The main reason to introduce such a large source list is the upcoming Planck mission[2]. There is very little radio data for the faint IBLs and HBLs. We have no real conception of their behaviour in the high radio frequencies, which is precisely the domain Planck is targeting. Our objective is to get some hands-on experience about the detectability of the faint BLO population to complement the theoretical studies on the subject (Giommi & Colafrancesco 2004; Giommi et al. 2006)

3.2 Results

We will shortly publish our BLO data at 37 GHz obtained between 2001 December and 2005 April (Nieppola et al. 2006b). The database consists of more than 3000 datapoints. Unfortunately, due to the nature of our our source sample the majority of the data are $S/N > 4$ upper limits. Overall, we were able to detect 34% of the sample at $S/N > 4$. Because of the relative radio brightness of LBLs, as much as 77% of them were detected. For IBLs and HBLs the percentages are 37% and 15%, respectively.

The most observed sources are some of the best-known BLOs, like OJ 287, Mrk 421, S5 0716+714, BL Lac and AO 0235+164. While these sources have tens or even hundreds of datapoints, the large majority of the sample does not. In fact, 96% of the sample was observed less than 10 times.

We studied the variability amplitudes by calculating variability indices. Fig. 4 shows the distribution of the index

[2]http://www.rssd.esa.int/Planck

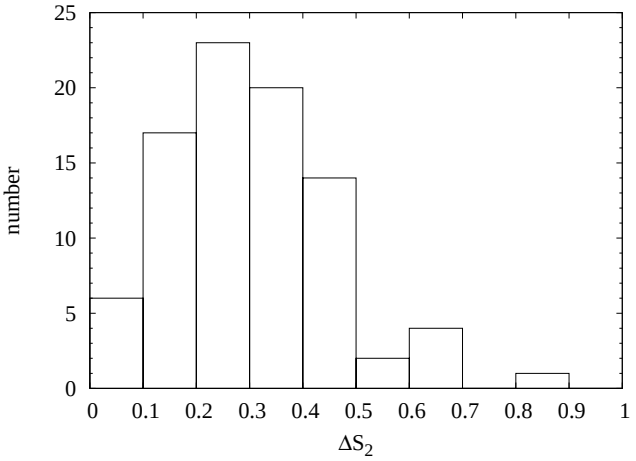

Figure 4: The distribution of the variability index $\Delta S_2 =$.

$$\Delta S_2 = (S_{max} - S_{min})/(S_{max} + S_{min}). \quad (1)$$

We see that most of the sources exhibit considerable variability. The distributions peaks in the interval 0.2-0.3. The object with $\Delta S_2 = 0.9$ is S5 0716+714, which underwent an unprecedented radio flare in 2003 (Ostorero et al. 2006).

Although HBLs and IBLs (XBLs) are typically hard to detect, our study shows that they can exceed the detection limit of Planck, which is comparable to that of Metsähovi. Many of the XBL detections occurred after several non-detections on the same source. A good example of this is RXS J1110.6+7133. It has 6 non-detections and one clear detection of 0.74 Jy. This suggests that the faint BLOs exhibit similar flaring as their radio-bright counterparts, being at times luminous enough for us to detect. To get an idea of the probability of such a serendipitous detection, we calculated the ratio of detections vs. non-detections for XBLs. It was of the order of 20%. Thus, roughly speaking, every fifth time we observe a thought-to-be-faint BLO, we actually get a detection at $S/N > 4$.

4 Future

Currently we are preparing a paper on the long-term radio variability of a limited sample of bright BL Lacs. It will continue the work done in Hovatta et al. (2006), focussing on the BL Lacs with more detail. We will also continue our work on the SEDs. So far we have only studied the apparent properties of the sources. Next we will take into consideration the relativistic effects caused by beaming, and examine the true, intrinsic properties and their possible differences between classes.

Acknowledgements. The authors made use of the CATS database (Verkhodanov et al. 1997) of the Special Astrophysical Observatory.

5 References

Bondi, M., Marchã, M.J.M., Dallacasa, D. & Stanghellini, C.: *MNRAS*, 2001, **325**, 1109.
Fossati, G., Maraschi, L., Celotti, A., Comastri, A. & Ghisellini, G.: *MNRAS*, 1998, **299**, 433.
Ghisellini, G.: *ApL&C*, 1999, **39**, 17.
Giommi, P., Ansari, S.G. & Micol, A.: *A&AS*, 1995, **109**, 267.
Giommi, P., Ghisellini, G., Padovani, P. & Tagliaferri, G.: *AIPC*, 2001, **599**, 441.
Giommi, P. & Colafrancesco, S.: *A&A*, 2004, **414**, 7.

Giommi, P., Piranomonte, S., Perri, M. & Padovani, P.: *A&A*, 2005, **434**, 385.
Giommi, P., Colafrancesco, S., Cavazzuti, E., Perri, M. & Pittori, C.: *A&A*, 2006, **445**, 843.
Hovatta, T., Tornikoski, M., Lainela, M. et al.: *A&A*, 2006, in preparation.
Jannuzi, B.T., Smith, P.S. & Elston, R.: *ApJ*, 1994, **428**, 130.
Kollgaard, R.I.: *VA*, 1994, **38**, 29.
Laurent-Muehleisen, S.A., Kollgaard, R.I., Feigelson, E.D., Brinkmann, W. & Siebert, J.: *ApJ*, 1999, **525**, 127.
Nieppola, E., Tornikoski, M. & Valtaoja E.: *A&A*, 2006a, **445**, 441.
Nieppola, E., Tornikoski, M. Lähteenmäki, A. et al.: *AJ*, 2006b, in press.
Padovani, P., Perlman, E.S., Landt, H., Giommi, P. & Perri, M.: *ApJ*, 2003, **588**, 128.
Padovani, P. & Giommi, P.:t *ApJ*, 1995, **444**, 567.
Ostorero, L., Wagner, S.J., Gracia, J. et al.: *A&A*, 2006, **451**, 797.
Sambruna, R.M., Maraschi, L. & Urry, C.M.: *ApJ*, 1996, **463**, 444.
Stein, W.A., O'Dell, S.L. & Strittmatter, P.A.: *ARA&A*, 1976, **14**, 173.
Teräsranta, H., Tornikoski, M. & Mujunen, A.: *A&AS*, 1998, **132**, 305.
Verkhodanov, O.V., Trushkin, S.A., Andernach, H. & Chernenkov, V.N.: *ASPC*, 1997, **125**, 322.
Veron-Cetty, M.P. & Veron, P.: *ESO Sci.Rep*, 2000, **19**, 1.

Host galaxy subtraction in differential aperture photometry

K. Nilsson[1], L. O. Takalo[1], M. Pasanen[1], E. Lindfors[1], A. Berdyugin[1] & S. Ciprini[1,2]

[1]Tuorla Observatory, University of Turku, Väisäläntie 20, FIN-21500 Pikkiö, Finland
[2]INFN Perugia & Physics Dept., University of Perugia, via Pascoli, 06123 Perugia, Italy

Abstract

Due to its simplicity and reliability, differential aperture photometry is widely employed to measure fluxes of variable sources, including blazars. However, the presence of a strong host galaxy component can make it difficult to compare measurements made by different observers, if e.g. different aperture radii have been used. We have studied the effect of aperture radius and seeing on 16 BL Lacertae objects currently monitored at Tuorla Observatory. We use simulated object fields for this purpose and take also into account any nearby stars and galaxies that might contribute light into the measurement aperture. Using this method we can correct measurements made with different aperture radii into the same aperture with an accuracy of $\sim$ 5-7% in the case of Tuorla monitoring data.

1 Introduction

The optical fluxes of blazars are most commonly measured from CCD images in differential photometry mode, i.e. by comparing the blazar brightness to the brightness of several calibrated comparison stars in the CCD image of the object. In this way changes in sky transparency can be eliminated and accuracies $< 1\%$ attained even under varying non-photometric conditions. The measurements are usually made using aperture photometry, i.e. by integrating the light inside a circular aperture, whose radius is determined by the angular extent of the source and by the seeing conditions.

The presence of a strong host galaxy component can affect differential aperture photometry at least in two ways. Firstly, the host galaxy adds unwanted flux to the measurement aperture, and the amount of the additional flux depends on the aperture radius. Thus it is difficult to compare observations between different observers if the measurements have not been made using the same aperture radius. For instance, in 1ES 2344+514 $\sim$ 80 % of the total R-band flux inside 5 arcsec radius arises from the host galaxy. Secondly, as discussed by Carini et al. (1991) and Cellone et al. (2000),

Table 1: The objects in this study.

1ES 0033+595	1ES 0120+340	RGB 0214+517
1ES 0806+524	1ES 1011+496	Mrk 421
Mrk 180	RGB 1136+676	1ES 1218+304
RGB 1417+257	1ES 1544+820	Mrk 501
OT 546	1ES 1959+650	BL Lac
1ES 2344+514		

seeing changes during the observations may introduce false variability in objects with a prominent host galaxy component. This is due to the fact that stars and galaxies have different surface brightness profiles and thus they respond differently to changes in the FWHM. This effect is generally not very strong (0.01-0.03 mag; Cellone et al. 2000), but it may nevertheless affect e.g. studies that look for very low-level intranight variability. The seeing effect is further amplified by the presence of nearby stars and galaxies, whose flux may leak into the measurement aperture in a seeing-dependent manner.

The purpose of this study was to determine the host galaxy contribution as a function of aperture radius and seeing for 16 BL Lacertae objects we are currently monitoring in the R-band at Tuorla Observatory (see Table 1). These BL Lacs were selected from the list of potential TeV emitters by Costamante & Ghisellini (2002) with the only selection criterion being $\delta > +20°$. About 4 years of monitoring data have been obtained by now.

2 Analysis

Our method of estimating host galaxy contribution consists of four steps: 1) obtain a deep high-resolution image of the object and fit a two-dimensional nucleus + host galaxy model to it. 2) Create a simulated image of the object field with a proper comparison star sequence, nearby sources and the object *without* the nuclear component. 3) select the PSF shape and FWHM and and convolve the image with the selected PSF. 4) Perform differential aperture photometry of the simulated image over a range of apertures and seeing conditions using the same parameters and procedures as for the real monitoring data. The resulting magnitudes should then correspond to the source flux in the absence of the nuclear component, i.e. the aperture correction.

For the imaging and model fitting part we used our existing analysis of R-band images obtained at the NOT during 1995-2005 (see e.g. Nilsson et al. 2003), or images kindly provided by R. Falomo, complemented by model fitting of any nearby stars and galaxies not analyzed before. In short, the model fitting separates the host galaxy contribution from the nuclear

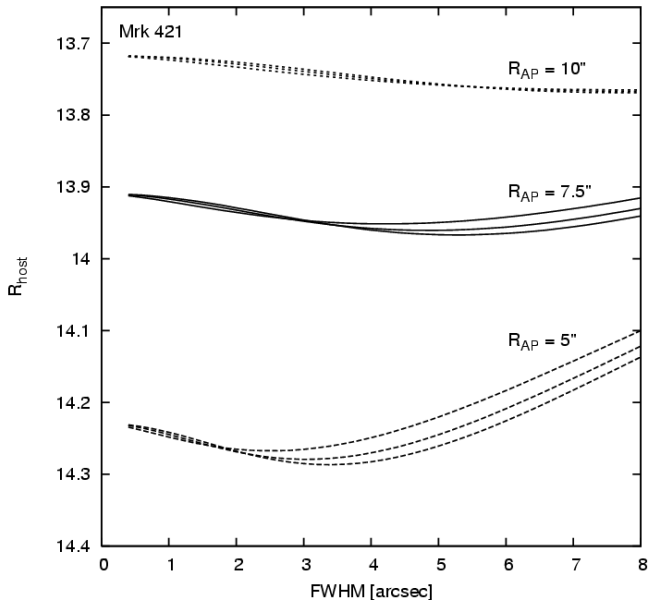

Figure 1: The R-band magnitude of the host galaxy of Mrk 421 as a function of seeing and three aperture radii. Note that the curves include also the effect of the companion galaxy 13 arcsec away.

contribution and enables an accurate two-dimensional model of the host galaxy to be created (see Nilsson et al. 1999 for details). We then created a photometric model of the field that included the host galaxy, any significant nearby companions and properly scaled comparison stars. This model was then convolved with three different Moffat profiles with $\beta = 2.0$, 2,5 and 3.0 over a grid of FWHM values from 0.5 to 8.0 arcsec. Finally, the simulated host galaxies were measured using the same procedures and software as the Tuorla monitoring data using aperture radii from 0.5 to 10.0 arcsec.

3 Results

Fig. 1 shows a typical example of the results obtained by the above procedure. As can be seen, the measured magnitudes depend more strongly on the aperture radius than on the FWHM. The effect of PSF shape is minor, although it must be noted that the PSF shapes considered here are quite similar to each other. In real data many PSF shapes are possible and the scatter due to this very likely larger.

The accuracy of the method depends mainly on the accuracy of the photometric calibration and on how accurately our model fits have been able to separate the host galaxy and nuclear contributions. The accuracy of the former can be estimated to be 0.02-0.05 mag, depending on the source. The latter error is much harder to estimate. Instead of trying to derive

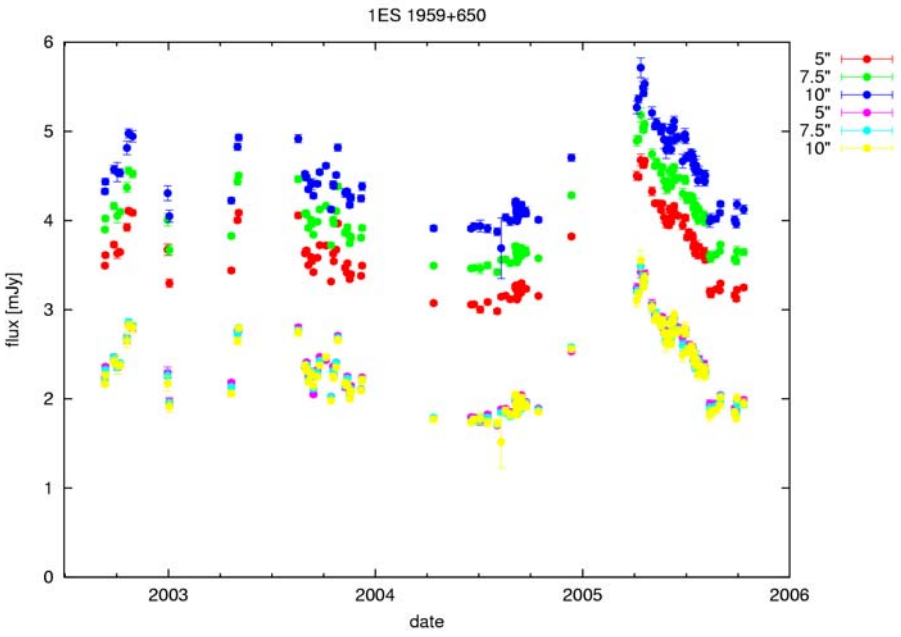

Figure 2: The light curve of 1ES 1959+650 measured with three different aperture radii before (upper curves) and after (lower three curves) applying the correction derived in this study.

rigorous confidence limits for every possible aperture, we have applied our method to real monitoring data and investigated possible systematic shifts that might appear due to errors in our method.

We measured our ∼4 years of monitoring data of all 16 sources with three different aperture radii, 5.0, 7.5 and 10.0 arcsec using differential photometry. As can be expected, larger apertures produced higher average brightness levels for sources with a bright host galaxy (see the upper three curves in Fig. 2). We then measured the FWHM in each monitoring frame by fitting a β=2.5 Moffat profile to stellar images and determined the respective host galaxy magnitude, which was then subtracted from each monitoring data point.

An example of the resulting light curves is shown in Fig 2 (the lower three curves). The average levels in the corrected curves generally agree very well, showing that our correction curves have no large systematic errors. The difference between average levels of corrected 5 arcsec curves and 7.5 arcsec curves was 5% on average for all 16 sources (total range from 0% to 13%). For the average levels of 5 arcsec and 10 arcsec curves the corresponding number was 7% (2% to 17%). These numbers give an idea of the average accuracy of our correction method using realistic monitoring data. Although the error is not large, it is still more advisable to ensure that the same aperture radius is used by all observers in monitoring campaigns, rather than trying to correct the differences afterwards.

4 Future work

Since the spectral shape of the blazar nucleus (e.g. the spectral slope) is often of great interest, the present work should be expanded to other wavelengths. Unfortunately, the high-resolution imaging data is very much confined to the red wavebands and hence a relatively big imaging effort is needed to achieve this. In addition, despite of the difficulty of estimating the error bars for the correction tables, this should be done to identify the regions in the FWHM-aperture radius space where the errors might be large.

Acknowledgments The authors thank R. Falomo for providing R-band images of three sources.

References

Carini, M. T., Miller, H. R., Noble, J. C., & Sadun, A. C. 1991, AJ, 101, 1196
Cellone, S. A., Romero, G. E., & Combi, J. A. 2000, ApJ, 119, 1534
Costamante, L., & Ghisellini, G. 2002, A&A, 384, 56
Nilsson, K. et al. 1999, PASP, 111, 1223
Nilsson, K. et al. 2003, A&A, 400, 95

Helical magnetic field models for parsec-scale radio jets

Andreas Papageorgiou, C.I.T., Cork, Ireland

Introduction

Constant development of VLBI techniques over many years meant that polarization observations of ever increasing quality and sensitivity could be made, allowing for transverse structure in jets to be studied in well resolved sources. Although there has, as yet, been no systematic study of jet profiles of transverse structure, we note the following features in some prominent jets from observations presented in here and in the literature:

i. Asymmetric distribution of total and polarized intensity across the jet (profile of 4C71.07 and 3C380 – fig. 1).
ii. Misalignment of the total and polarized intensity maxima in *I* and *P* profiles across the jet. In cases, the misalignment can be in the order of 1/3 of the beam. (profile of 4C71.07 and 3C380 – fig. 1).
iii. Edge brightening in total intensity and polarization. (3C 353, Swain, Bridle & Baum 1998)
iv. Projected magnetic field flips from longitudinal to transverse across the jet. (e.g. 1055+018, Attridge et al. 1999).

One proposed mechanism to explain these features is through interaction with an external cloud (e.g. Attridge et al.1999). According to this model, the edge brightening can be attributed to compression at one side of the jet while the change of the projected magnetic field from transverse to longitudinal is due to sheering. However this model fails to explain observed displacements of the *I* and *P* maxima. In addition, it is not clear how such asymmetries, arising from external medium interaction, could be sustained for long as the jet progresses. Considering the small angles to the line of sight that jets have and the relativistic velocities involved, interaction with an external medium would cause the jet to deflect, which would most likely be projected as a sharp bend in the observer's frame, but such large bends are not seen in 4C 71.07, 1055+018 or 3C 380 in regions where such asymmetries occur.

Alternatively, the features mentioned above are qualitatively similar to predictions by models of jets where the jets are considered to be tubes of synchrotron emission, threaded by magnetic fields of helical geometry. In these models, asymmetries in the total and polarized intensity profiles can arise because of the way a helix is projected.

The main advantage of such models is that they can produce all of the observed features mentioned above while avoiding any physical asymmetries (such as pressure asymmetries) which might cause the jet to deflect or possibly destabilize.

Helical magnetic field models of jets have been considered several times in the past (e.g. Fomalont et al. 1980, Chan & Henriksen 1980, Laing 1981) however at the time there were no polarization observations on these scales, of sufficient resolution and sensitivity, to test the models. Since then, very little work has been done on the idea of helical magnetic fields threading jets (MHD simulations by Clarke et al., 1989 or modelling the transverse structure of the VLA scale jet in 3C353 with a helical field, Swain, Bridle & Baum 1998).

It is only recently that helical magnetic fields are being considered again, this time prompted by observations of Faraday Rotation Measure (RM) across the jet. Asada et al. (2002) showed a RM profile of the jet in (3C273) which had a sinusoidal form, which they attributed to the presence of a helical magnetic field. Based on the same idea, Gabuzda, Murray & Cronin (2004) published similar results on four different sources proposing that helical magnetic fields in these jets could account for the observations.

This work presents total and polarized intensity profiles as well as distributions of projected magnetic fields predicted by helical magnetic field models. The profiles are compared to profiles from observations of 4C 71.07, 3C 380, 1928+738 and 1055+018.

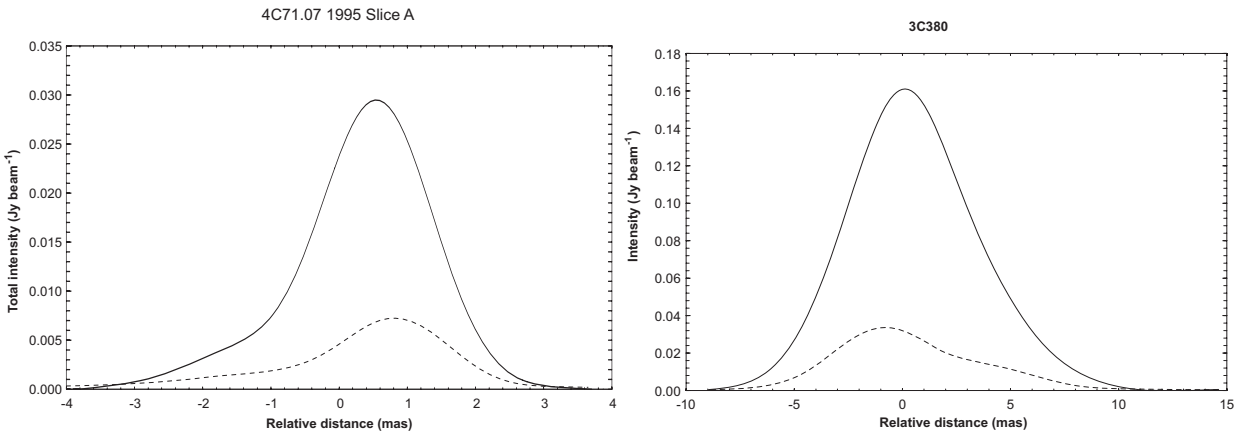

Figure 1: Left: 8GHz total and polarized intensity transverse profile of 4C71.07 (1995.7), 6 mas away from the core. Convolution beam is ~ 1.5 mas. Right: 5GHz total and polarized intensity transverse profile of 3C380, 16 mas away from the core. Convolution beam is ~ 4 mas. Solid line corresponds to total intensity and dashed line corresponds to polarized intensity with longitudinal magnetic field

Models for helical fields

The model used to produce the total and polarized intensity profiles is based on the model proposed by Laing (1981). Additional parameters were included in an attempt to account for Laing's model shortcomings when compared with actual data.

The model approximates parsec-scale radio jets by a cylinder (i.e. zero opening angle). The cylinder is filled with a uniform, isotropic distribution of electrons which emit optically thin synchrotron radiation:

$$N(E)dE \propto E^{-(2\alpha+1)}dE \tag{1}$$

where α is the spectral index of the power-law distribution. For simplicity, a value of α=1 is used rather than the value of α~ 0.7 typical for optically thin synchrotron emitting regions. This is a good approximation since the model fractional polarization changes only by a few percent for spectral index values in the range of 0.7 to 1 (Laing 1981).

The emission properties of a point in the cylinder can then be calculated using the Stokes parameters while assuming that there is negligible circularly polarized emission (V=0). At any point in the cylinder, the synchrotron emissivity ε (and therefore the intensity, I) is given by (Pacholczyk 1970):

$$\varepsilon \propto B^{\alpha+1}\left|\sin\theta\right|^{\alpha+1} \tag{2}$$

where B is the magnetic field strength, α is the spectral index and θ is the angle between the field and line of sight. Given that that the radiating electrons are distributed uniformly in the cylinder, the Stokes parameters for an E-W jet are:

$$\begin{aligned} I &= C(B\sin\theta)^{\alpha+1} \\ Q &= p_o I\cos 2\chi \\ U &= p_o I\sin 2\chi \end{aligned} \tag{3}$$

where C is a constant, p_o is the maximum possible fractional polarization (p_o=(3α+3)/(5α+3)) and χ is the angle (measured anticlockwise) between the polarization E-vector and the North-South axis on the plane of the sky, which is also equal to the angle of the projected magnetic field minus 90°.

The projected emission properties of the cylinder can then be obtained by integrating the Stokes parameters along the intersection of the cylinder and the line of sight giving:

$$\begin{aligned} I &= I_{Int} \\ P &= \left(Q_{Int}^2 + U_{Int}^2\right)^{1/2} \\ \chi &= \frac{1}{2}\tan^{-1}\frac{U_{Int}}{Q_{Int}} \end{aligned} \tag{4}$$

Equations 3 and 4 can be used to calculate the emission properties of different geometries of magnetic field.

Simple Helical field model

The Simple Helical field has been proposed and had its emission properties explored by Laing (1981). In this model the magnetic field threading the cylinder has a helical geometry with the pitch angle of the helix and the strength of the magnetic field remaining constant with distance from the cylinder axis. Laing derived analytical solutions for the case of α=1:

$$I_{SH}(x) = \frac{CB^2}{\sin\delta}\left[a\left(1-\cos^2\gamma\cos^2\delta\right)+b\sin 2\gamma\sin 2\delta - c\sin^2\gamma\sin^2\delta\right]$$
$$Q_{SH}(x) = \frac{p_o CB^2}{\sin\delta}\left[a\left(\sin^2\gamma-\cos^2\gamma\sin^2\delta\right)+b\sin 2\gamma\sin 2\delta - c\sin^2\gamma\left(1+\cos^2\delta\right)\right] \quad (5)$$

where I_{SH} and Q_{SH} are the I and Q Stokes parameters predicted by the Simple Helical model, γ is the helix pitch angle (γ=90° corresponds to toroidal field), δ is the angle between the cylinder axis and the line of sight (both γ and δ are in the jet frame), p_o = 0.75 and:

$$a = \left(1-\frac{x^2}{R^2}\right)^{1/2}, \quad b = \frac{x}{2R}\ln\left|\frac{1+a}{x/R}\right| \quad \text{and} \quad c = \frac{|x|}{R}\cos^{-1}\frac{|x|}{R}$$

where R is the radius of the cylinder and x is the projected distance from the cylinder's axis. Note that the solution of $Q_{SH}(x)$ in equation 5 has been corrected for a misprint that appears in Laing's solution.

Because sin2χ is antisymmetric, the integral of U along the line of sight is always 0 thus giving:

$$P(x) = |Q(x)|$$
$$\chi = \begin{cases} 90^\circ \text{ for } Q > 0 \\ 0^\circ \text{ for } Q < 0 \end{cases} \quad (6)$$

or alternatively, the projected magnetic field is transverse for Q>0 and longitudinal for Q<0.

Figure 2 shows profiles of total intensity, I, and polarized intensity, P, for different values of γ and δ. Looking at the profiles, several important features need to be noted:

i. The distribution of total and polarized intensity is generally asymmetric, except in the case of toroidal magnetic field (γ=90°) or angle to the line of sight perpendicular to the cylinder axis (δ=90°).
ii. There are instances where there is a significant displacement between the I and P maxima. (e.g. for γ=30° and δ=60°).
iii. The fractional polarization varies considerably across the profile. In cases the fractional polarization profile decreases at the centre of the profile (e.g. for δ=30° and γ=30° polarization becomes zero at the centre).
iv. The polarized intensity distribution can have either one, two or three local maxima. Also the orientation of the projected magnetic field can have one of the following configurations: a) longitudinal all across the profile, b) longitudinal on one side and transverse on the other, c) transverse field enveloped by longitudinal and d) transverse all across (in cases where longitudinal field at the edges is very small, e.g. for γ=90° and δ=60°).

The Simple Helical model predicts intensity and polarization distributions with easily distinguishable features similar to those mentioned in the Introduction. For example, at first look, the I and P distributions for γ=30° and δ=60° (fig. 2) show similar asymmetry, displacement of the I and P maxima and projected magnetic field (longitudinal) as the profile obtained from 4C 71.07 (fig. 1). Also for γ=60° and δ=60° the I and P distributions resemble those seen in the jet of 1055+018 (Attridge et al. 1999).

Additional parameters

Even though the purely helical model can reproduce the observed features mentioned in the Introduction, closer comparison with observed profiles reveals several shortcomings. In particular, fractional polarization predicted by the model is higher than what is usually observed. In addition, the polarized intensity predicted by the model increases quite slowly at the edges, compared to the data.

In order to account for these discrepancies, the helical geometry has been enhanced with several modifications, which are discussed in the following paragraphs.

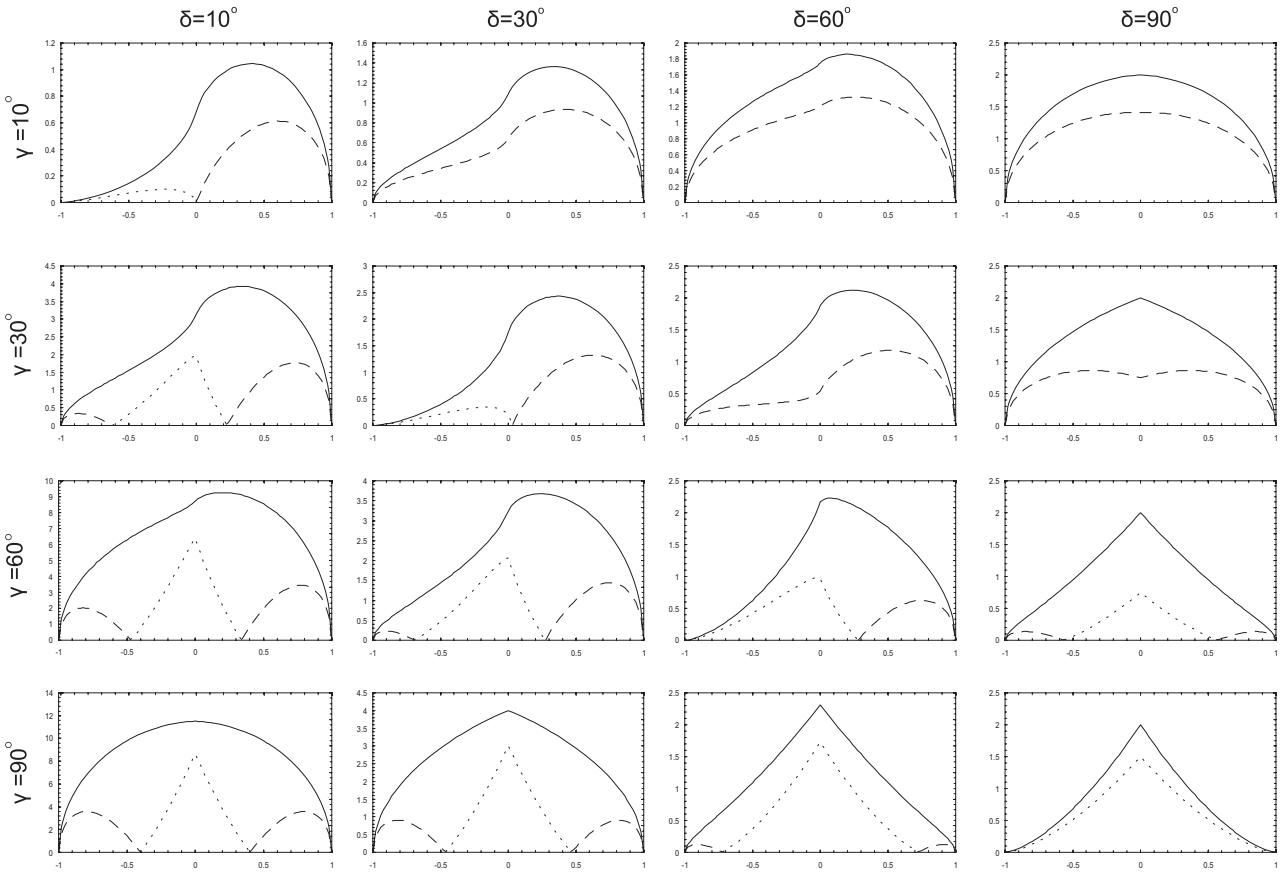

Figure 2: Transverse (across the jet) structure produced by the helical model, for different values of angle to the line of sight, δ, and helix pitch angle, γ. Solid lines correspond to total intensity. Dashed and dotted lines correspond to polarized intensity where the projected magnetic field is longitudinal or transverse respectively.

Tangled magnetic field component

The overall fractional polarization predicted by a purely helical model is quite high, often reaching the theoretical maximum of 75 percent (for α=1). This is in disagreement with real observations, where fractional polarization is smaller, with typical values ranging from a few percent up to 35 percent. In an attempt to account for that, a certain amount of disorder was superimposed on the helical geometry in the form of tangled magnetic field. The reason for this addition is the fact that synchrotron emission from a tangled magnetic field produces no polarization, assuming that the scale of entanglement is much smaller than the resolution of observation.

In physical terms, a partly helical, partly tangled magnetic field can be considered as a small volume of purely tangled magnetic field being elongated on the local direction of the helix. The magnetic field can then be expressed in the following form:

$$\frac{\left\langle B_t^2 \right\rangle}{\left\langle B_{Hel}^2 \right\rangle} = \frac{f}{1-f} \tag{7}$$

where, f is the fraction of the magnetic field energy density in tangled form.

So, the synchrotron emission coefficient from such a magnetic field is:

$$\varepsilon_{Tot} = \left\langle \varepsilon_t \right\rangle + \varepsilon_{Hel} \tag{8}$$

where the brackets denote the average over all angles.

For a cell with purely tangled magnetic field:

$$\left\langle \varepsilon_t \right\rangle = \int_0^{\pi} \left[C\left(f^{1/2} B \sin\theta \right)^{1+\alpha} \right] \frac{2\pi \sin\theta}{4\pi} d\theta \tag{9}$$

where C is the same constant as equation 5, and θ is the angle on the plane of the sky made by an element of the magnetic field in the cell..

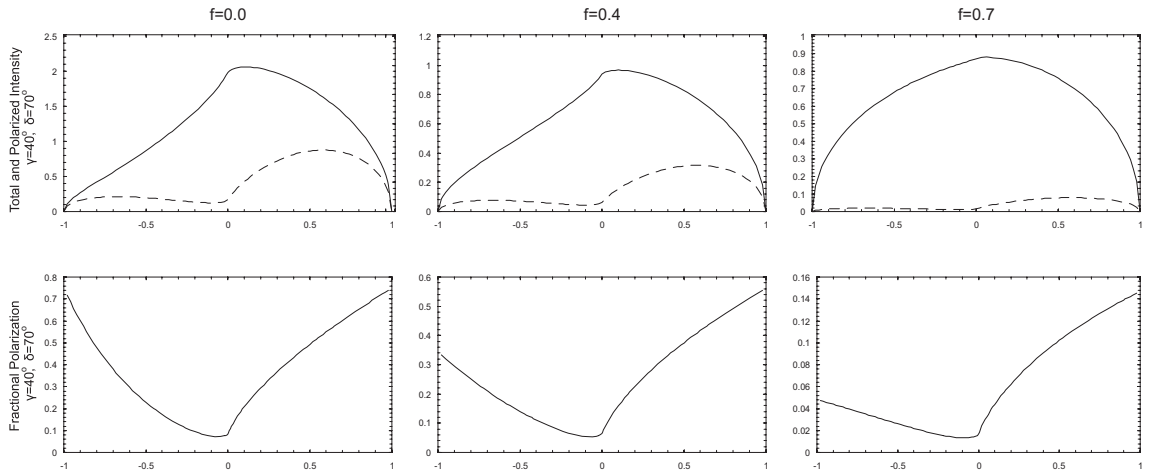

Figure 3: Effect of the tangled magnetic field component on the Simple Helical geometry The plots show different contributions of f to the Simple Helical geometry (γ=40°, δ=70°). Left: Plots of total intensity (solid line) and polarized intensity (dashed line). Right: Fractional polarization.

For the case where α=1, equation 9 gives:

$$\langle \varepsilon_t \rangle = \frac{2}{3} CfB^2 \tag{10}$$

The total intensity distribution of a partly helical, partly tangled geometry can be obtained by integrating equation 8 along the line of sight:

$$I(x) = \frac{2}{3} CfB^2 \frac{2\sqrt{R^2 - x^2}}{\sin\delta} + (1-f) I_{SH}(x) \tag{11}$$

Since the tangled component does not contribute to polarization:

$$Q(x) = (1 - f) Q_{SH}(x) \tag{12}$$

where $I_{SH}(x)$ and $Q_{SH}(x)$ are the solutions for the purely helical geometry.

Figure 3 shows the effect of the tangled magnetic field component for different values of f. As expected, the fractional polarization decreases noticeably with increasing values of f. Another effect of the tangled component is that it reduces the asymmetry in the total intensity distribution, making it more semicircular, as the first term in equation 11 becomes more dominant.

Radial compression

Another problem with the helical geometry is that fractional polarization in the model falls more rapidly at the edges than in observations. Figure 4 shows an example of this; it displays a comparison between the helical field model and a profile obtained 6 mas away from the core in the jet of 4C71.07.

In order to account for this discrepancy, the helical model needs to be modified in such a way that fractional polarization increases at the edges but remains unaffected in the middle. One way to achieve that, is to consider the possibility of a tangential (two-dimensional) compression of the outer radiating shell of jet. Even though there is no observational evidence to support such behaviour, it is considered here a reasonable assumption since radio jets expand into a medium of higher density as they propagate outward. The reason that this geometry is being considered is because a volume of purely tangled field compressed in one dimension displays a range of fractional polarization values, depending on the viewing angle; when observed along the direction of compression, polarization is zero, while when observed along the plane of compression, polarization takes a maximum value, depending on the degree of compression.

For the production of total and polarized intensity profiles of this configuration, the emissivity of the two component magnetic field (helical and tangled) needs to be determined as a function of the compression factor, k. For the tangled component, the emission coefficient is given by Hughes, Aller & Aller (1985):

$$\varepsilon_t \propto \frac{B_t^2}{3k^2} \left(2 - \sin^2\psi\left(1 - k^2\right)\right) \tag{13}$$

where, ψ is the angle between the line of sight and the plane of compression normal.

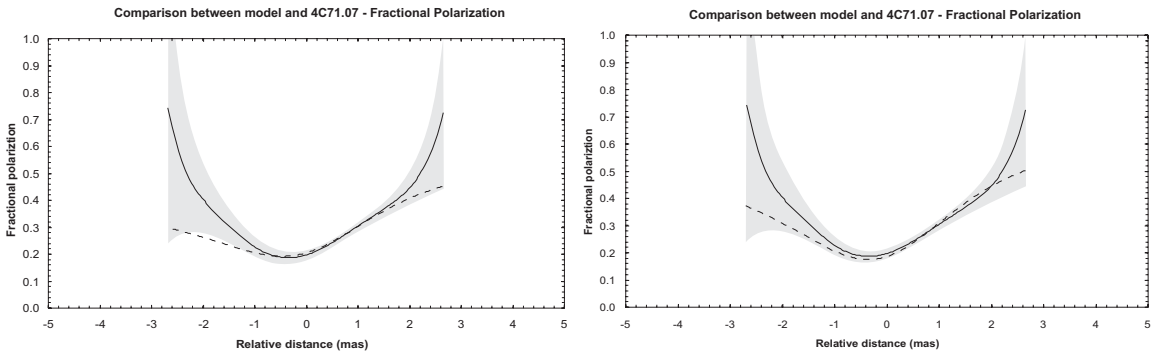

Figure 4: Comparison of fractional polarization between 4C71.07 and model. Left: the model includes only helical geometry and the tangled magnetic field component. Right: the model includes helical geometry, tangled component and radial compression.
Solid line corresponds to the data. Dashed line corresponds to model. Shaded area corresponds to fractional polarization uncertainty of the data.

For the emissivity of the helical component:

$$\varepsilon_{Hel} \propto N' B'^{1+\alpha} \tag{14}$$

where, N' is the number of synchrotron electrons after compression and B' is the magnetic field strength after compression.

For synchrotron power-law energy distribution:

$$N(E_o)dE_o = N_o E_o^{-(2\alpha+1)} dE_o = N' E'^{-(2\alpha+1)} dE'$$

$$N' = N_o \left(\frac{E_o}{E'} \right)^{-(2\alpha+1)} \frac{dE_o}{dE'} \tag{15}$$

Assuming adiabatic compression, for one-dimensional compression the total electron density is proportional to k^{-1}. Hence:

$$\frac{E_o}{E'} \propto k^{1/3} \text{ and } \frac{dE_o}{dE'} \propto k^{1/3} \tag{16}$$

Hence equation 15 gives: $N' = N_o k^{-\frac{2\alpha}{3}}$.

For one-dimensional compression of a uniform magnetic field:

$$B \propto k^{-1} \tag{17}$$

The helical field emissivity (equation 14) varies with k as:

$$\varepsilon_{Hel} \propto k^{-8/3} \quad (\text{for } \alpha=1) \tag{18}$$

Equations 13 and 18 can be used to calculate the emission properties of regions of radial compression.

Comparison with observations

Transverse profiles of total and polarized intensity, as well as fractional polarization and χ were obtained from observations of jets. The profiles were taken from regions between knots where the jet appears to be extending outward in a straight line. These profiles are used for comparison with predictions from the models.

Comparison method

In order for the model I and P profiles to be compared with profiles from real sources, they first need to be convolved with a two-dimensional Gaussian beam, equivalent to that of the observed profile. The model profiles also need to be scaled in both axes, since they are both in arbitrary units. Intensity scaling (y-axis) is simply done by multiplying the model intensity so that its maximum is equal to that of the observed profile. For the relative position (x-axis), scaling is done by matching the positions of local I and P maxima of the post-convolved model profiles and the observed profiles. In cases where the profiles have only one maximum, points of curvature inversion are also taken into account. Because the size of the convolving Gaussian can affect the relative position of the resulting maxima, determination of the full-width-at-half-

maximum (FWHM) of the Gaussian is an iterative process. The FWHM is successfully determined when the ratio of FWHM to the distance between two distinguishable features (e.g. maxima) in the model profiles is equal to the observed equivalent.

Determination of the best fit to the observed data was done by searching the parameter space of the model, which apart from the two main parameters, γ and δ (helix pitch angle and angle to the line of sight respectively) also includes parameters for the fraction of the magnetic field in tangled form, f and also the compression factor, k.

Due to the wide range of profile behaviours, the iterative way of determining the FWHM of the convolving beam and number of parameters, fitting the model to the data was done manually instead of using a fitting algorithm.

Individual sources

4C71.07

Figure 5 shows a comparison between the model and data obtained from an 8 GHz observation of 4C71.07. The model profiles were obtained for γ=40^o, δ=75^o, f=0.34 and k=0.6. The model reproduces the asymmetric distribution in polarized intensity, the displacement between the I and P maxima (0.5 mas, approximately a third of the convolving beam) and the overall degree of polarization. The inclusion of the radial compression had the desired effect of increasing the fractional polarization at the edges, although not sufficiently enough to compare well with the data.

3C 380

Figure 5 shows a comparison between the model and data obtained from a 1.6 GHz observation of 3C380. The model profiles were obtained for γ=40^o, δ=80^o, f=0.4. The model reproduces the asymmetric distribution in polarized intensity, the displacement between the I and P maxima (0.9 mas, a quarter of the convolving beam) and the overall degree of polarization.

1055+018

Figure 6 shows a comparison between the model and 1055+018 (5GHz). The intensity values and positions of the data were obtained from the contour plots published by Attridge et al. (1999). The model profiles were obtained for γ=60^o, δ=80^o, f=0.69. It can be seen that the model describes the polarized intensity and magnetic field orientation (predominantly transverse, longitudinal at the edge) fairly well; however, it fails to adequately account for the total intensity.

1928+738

Figure 6 shows a comparison between profiles from the model and 1928+738 (5GHz). The intensity values and positions of the data were obtained by summing the clean components across the jet. The model profiles were obtained for γ=48^o, δ=80^o, f=0.69.

Sensitivity of the model to the parameters

Figure 7 shows the sensitivity of the model to parameters γ and δ. In these plots the best fit obtained for 4C71.07 is superimposed to model plots of γ and δ plus and minus 3^o. It can be seen that small changes in γ can cause noticeable changes in fractional polarization as well as changing the shape of the polarized intensity profile. Changing δ has a less pronounced effect on fractional polarization but affects the shape of the polarized intensity profile in a similar way to changes in γ.

Figure 7 also shows how the model profiles are affected with changing k. The fractional polarization plot clearly demonstrates the effect that the radial compression was introduced for; to increase the fractional polarization at the edges without affecting it in the centre.

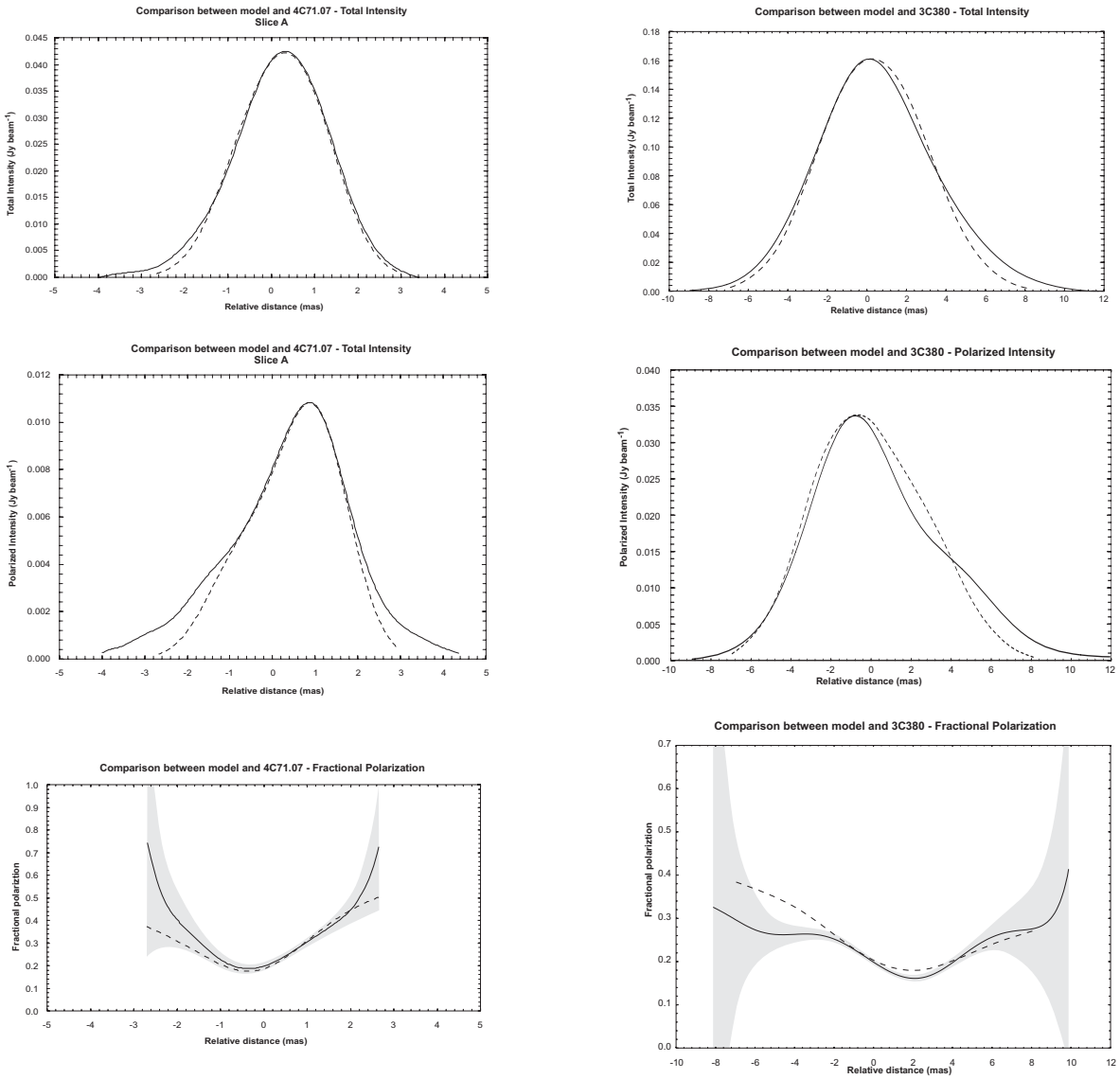

Figure 5: Left: Comparison between 4C71.07 (1997.9, 8GHz) and model. Parameters used: γ=40°, δ=75°, f=0.34, k=0.6 (the radial compression was applied to the outer 8 percent of the jet). I noise level: 2 mJy, P noise level: 3 mJy. Right: Comparison between 3C380 (1.6GHz) and the Helical Model. Parameters used: γ=40°, δ=80°, f=0.4 and no radial compression. I noise level: 2 mJy, P noise level: 2.2 mJy.
Top: Total intensity. Middle: Polarized intensity. Bottom: Fractional polarization Solid line corresponds to the data. Dashed line corresponds to model. Shaded area corresponds to fractional polarization uncertainty in the data.

Conclusion

Summary of results

- Studies of the transverse structure of jets reveal several interesting features such as asymmetry in the distribution of total and polarized intensity, displacement between the total and polarized intensity maxima, edge brightening and the projected magnetic field may flip by 90°. All these features can be explained by assuming that jets are threaded by magnetic fields of helical geometry.
- Comparisons between observations and a purely helical field model reveal that the purely helical field predicts too high fractional polarization. A degree of disorder (in the form of tangled magnetic field), is necessary to be introduced, in order to lower the model's fractional polarization to levels comparable to observations.
- Comparison between model and the jet in 4C71.07, revealed that while the model describes the emission at the centre of the jet, it fails to reproduce the sharp rise in fractional polarization seen at the edges. In an attempt to increase the model fractional polarization at the edges while leaving the centre unchanged, it was postulated that the jet's outer layer is radially compressed.

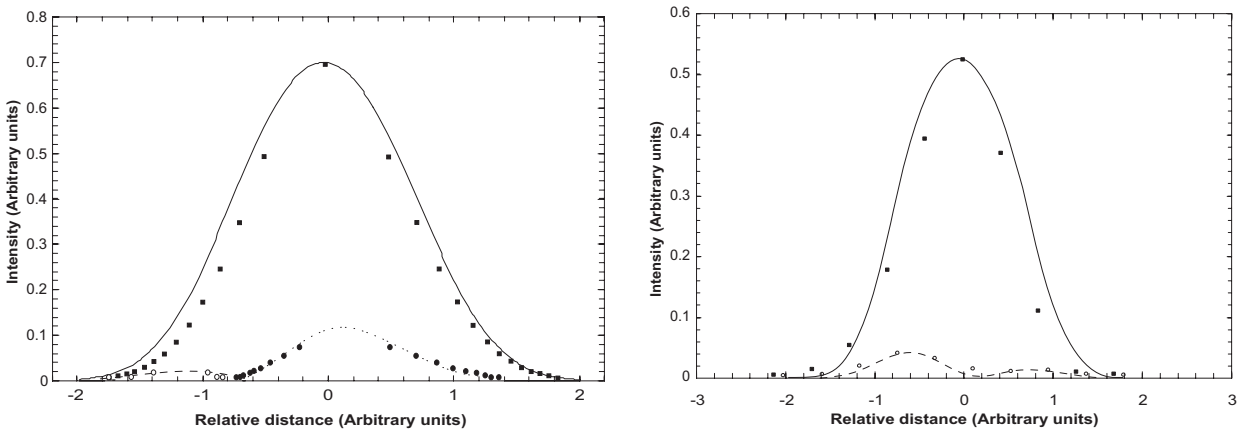

Figure 6: Left: Comparison between slice in 1055+018 (5GHz) and the Helical Model. Parameters used: γ=60°, δ=80°, f=0.69, k=0. I noise level: 1.7 mJy, P noise level: 0.5 mJy.
Right: Comparison between slice in 1928+738 (5GHz) and the Helical Model. Parameters used: γ=48o, δ=80o, f=0.69, k=0.
Solid line: total intensity, Dotted line: model polarized intensity with transverse magnetic field. Dashed line: polarized intensity with longitudinal magnetic field. Squares: data total intensity. White circles: data polarized intensity with longitudinal magnetic field. Black circles: polarized intensity with transverse magnetic field.

- For 3 out of 4 of the sources, the inferred magnetic field pitch angle lies in the region of 40 to 50 degrees. For the remaining source (1055+018) a pitch angle of 60° provided a good comparison. On the other hand there was no preference for the values of f (the fraction of magnetic field energy density in tangle form), which had values ranging from 0.26 to 0.76.

Discussion

In has been demonstrated that helical magnetic field geometries in jets can produce a wide range of behaviours in total intensity and polarization, which can be seen in observations of jets. Of course, due to its simplicity, the model is not expected to give an accurate description of highly complex and dynamic objects such as jets, instead it is meant to support the idea that helical magnetic field geometries are present and contribute to the emission structure of radio jets.

The helical field model produced a reasonable reproduction of the profiles from several of the sources presented here. However, the comparisons failed in several cases, in particular at the edges of the jet, signifying that the geometries considered here cannot be a complete solution to the magnetic field structures. Nevertheless, the model accounted for a number of observed features.

In particular the model managed to account for a range of different structures; the asymmetric polarized intensity distribution seen in 4C71.07 and 3C380 and 1928+738, as well as accounting for the displacements (ranging from one quarter to a third of the observation beam size) between the I and P maxima seen in these sources. In the case of 1055+018 the model described the double peak polarization distribution of the profile while at the same time accounted for the orientation of the projected magnetic field (predominantly transverse and longitudinal at the edge) and the position of the I and P maxima.

The structure observed in 1055+018 has been previously attributed to sheer due to interaction with external medium on the North side of the jet (Attridge et al. 1999). Even though this model can provide an explanation for the longitudinal magnetic field on one side of the jet it does not account for the rest of the observed features or the lack of a deflection of the jet.

An additional feature, radial compression, was also introduced. This was done in order to account for fractional polarization discrepancies at the edges of the jet where observed fractional polarization was usually higher than that predicted. Such a radial compression is considered here as a reasonable assumption, considering that jets expand radially in a denser medium. The compression used in this model (k= 0.6) was confined in the outer layer, 8 percent of the radius of the model jet. However, despite that the inclusion of the radial compression produced the desired effects, it still was insufficient to account for the discrepancy at the edges.

An interesting result is that all the predicted pitch angles, apart for one, lie in the region of 40 to 50 degrees. To some extent this is a selection effect since the jets presented here have predominantly longitudinal magnetic fields (with the exception of 1055+018 which gives pitch angle of 60°).

Further work

As already mentioned in the previous section, the model fails to give a complete description of the observations, particularly failing at the edges of the profiles by producing too little fractional polarization. Alternative geometries should also be examined, for example a helical field surrounded by a sheath of longitudinal field, a configuration that could arise as a result of interaction of the jet with the external medium.

The case of helical magnetic fields can be reinforced (or not) by Faraday rotation observations; observations of asymmetric Faraday rotation profiles across the jet have been attributed to helical magnetic field (Asada 2002, Gabuzda, Murray & Cronin 2004). Such models also make predictions of γ and δ providing an additional, independent way to test the possibility of helical fields and compare predictions from this work.

References

Asada K., Inoue M., Uchida Y., Kameno S., Fujisawa K., Iguchi S., Mutoh M., 2002, PASJ, 54, 39
Attridge J. M., Roberts D. H., Wardle J. F. C., 1999, ApJ, 518, 87
Chan K. L., Henriksen R. N., 1980, ApJ, 241, 534
Clarke D. A., Burns J. O., Norman M. L., 1989, ApJ, 342, 700
Fomalont E. B., Bridle A. H., Willis A. G., Perley R. A., 1980, ApJ, 237, 418
Gabuzda, D. C., Murray É., Cronin P., 2004, MNRAS, 351, 89
Hughes P. A., Aller H. D., Aller, M. F., 1985, ApJ, 298, 301
Laing R. A., 1981, ApJ, 248, 87
Pacholczyk A. G., 1970 in Radio astrophysics. Nonthermal processes in galactic and extragalactic sources, Freeman
Swain M. R., Bridle A. H., Baum S. A., 1998, ApJ, 507, 29

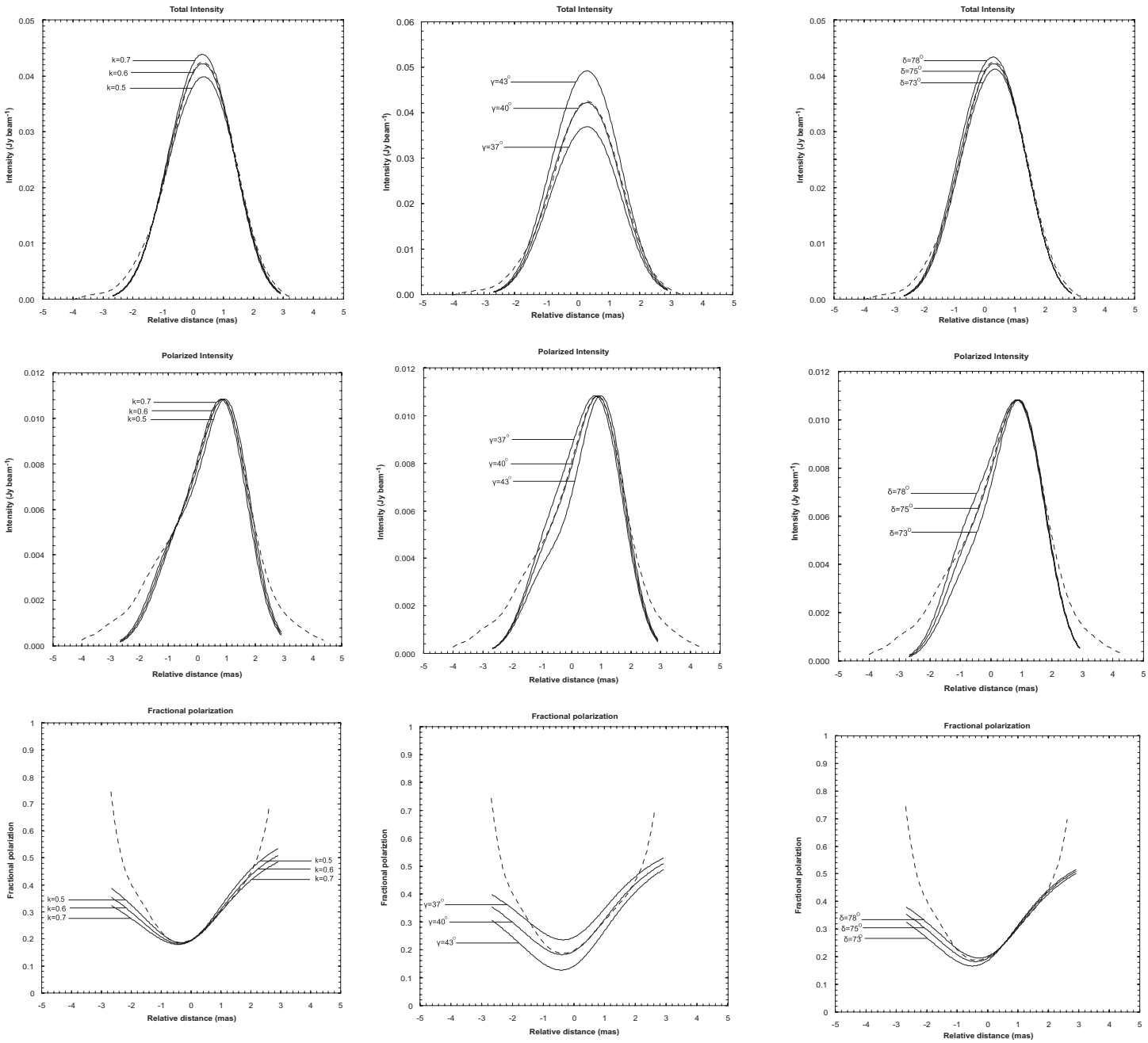

Figure 7: Left Column: Sensitivity of the 4C71.07 model fit to varying values of *k*. Middle column: Sensitivity of the 4C71.07 model fit to varying values of *γ*. Right column: Sensitivity of the 4C71.07 model fit to varying values of *δ*.
Dashed line: data. Solid line: Model. Parameters: γ=40°, δ=75°, f=0.34 and d=0.08.

GPS studies during the ENIGMA era

I. Torniainen[⋆], *M. Tornikoski*[⋆], *A. Lähteenmäki*[⋆], *M. F. Aller*[⋆⋆], *H. D. Aller*[⋆⋆], *M. G. Mingaliev*[⋆⋆⋆]

[⋆] Metsähovi Radio Observatory, Helsinki University of Technology
Metsähovintie 114, FIN-02540 Kylmälä, Finland
ilo@kurp.hut.fi
[⋆⋆] Department of Astronomy, University of Michigan
[⋆⋆⋆] Special Astrophysical Observatory of Russian Academy of Sciences

Abstract

We have studied two samples of gigahertz-peaked spectrum sources, one consisting of mostly quasars and the other consisting of galaxy-type objects. Among both samples most of the GPS sources lost their GPS status because with competent data sets the shape of the spectrum was not in compliance with a GPS spectrum. Instead a remarkable share of the quasars were actually flat-spectrum sources caught in a flare of which the spectrum is inverted. Also many of the galaxies did not have enough data for solid classifications so, with more observations at different frequencies, they can turn out to be anything from genuine GPS sources to flaring blazars with more observations at different frequencies.

This implicates a complicated situation for ESA's Planck mission. In order to study the anisotropies of the cosmic microwave background, the contribution of the foreground emission must be known. The different possibilities instead of classical invariable GPS sources will make predictions complex.

1 Introduction

Gigahertz-peaked spectrum (GPS) sources are active galactic nuclei which are characterized by a convex radio continuum spectrum peaking at the GHz-frequencies. Their nature is still unclear, but currently the generally accepted scenario suggests that at least s ome of them are newborn radio sources in which the activity has been triggered on only 100 - 1000 years ago (e.g. Mutel & Phillips 1988; Murgia et al. 1999). There are both quasar and galaxy type GPS sources, which have a similar shape of the spectrum but the nature and the physics are thought to be different. For a review of the GPS sources, see O'Dea et al. (1998).

Our motivation for studying the GPS sources emerged from the needs of the foreground science of ESA's Planck mission. In order to be able to distinguish the anisotropies of the cosmic microwave background, the contribution of the extragalactic radio sources must be eliminated. Since the major published all-sky surveys have been performed at low radio frequencies, the number and the nature of the sources visible at the Planck's frequency band (> 30 GHz) is unclear.

If only the steep-spectrum and flat-spectrum sources are considered, the sky would be quite easily predictable. However, the evidence for the high-peaking inverted-spectrum sources made us wonder how many and how bright sources it really will be able to detect.

2 First sample

Our first idea was to study if there were any high-peaking GPS sources in the Metsähovi monitoring sample. We collected radio data from the literature and constructed the radio continuum spectra for the entire Metsähovi sample. From the spectra we picked the most promising sources and also all the GPS, compact steep-spectrum (CSS) sources, and high frequency peakers (HFP) identified in the literature, as well as sources which had been associated with inverted spectrum before. The sample included 44 previously identified inverted-spectrum sources and 16 new candidates, mostly quasar-type objects. After two years of additional monitoring and collecting additional data from the literature, we studied the spectral indices, the fractional variability index, and the turnover frequency.

The results were different from what we originally anticipated. We had presumed that there would be a population of high-peaking sources but instead most of our candidates and the sources identified in the literature turned out to be very variable and to have inverted spectrum only during flares. Thus, no new GPS sources were found, and only five of the GPS sources from the literature still retained their consistent convex shape of the spectrum and low variability.

These results imply that genuine quasar-type GPS sources are rare, and most of the studied QSOs have been identified as GPS sources with insufficient monitoring and multi-frequency observations. Therefore also the results from the earlier studies should be taken with caution, since most of the sources are not what they have been assumed to be. Instead of a high-peaking inverted-spectrum source population there seems to be a great amount of sources whose spectrum is steep or flat at quiescent stages and strongly inverted during flares. The variability was rather high also among the genuine GPS sources. Our study and its results and conclusions are presented in detail in Torniainen et al. (2005).

3 Second sample

We then proceeded to study whether there was such contamination present also among the galaxy-type GPS samples. We collected most of the bright GPS galaxy samples from the literature, all together 96 sources, observed them and collected all possible radio data for them to study if there are incorrectly identified GPS galaxies. Our sample included both frequently monitored sources and sources with only a few detections.

The spectra of the sample show that only 30 % of the sources were definite or highly probable GPS sources, with fractional variability index $\mathrm{Var}_{\Delta S,MAX} < 3$ and spectral index below the turnover $\alpha_{below} > 0.5$. A remarkable share of the sources (29 %) had only a few data points, and with such insufficient data no classification should be done, no matter how perfectly convex the shape of the spectrum looks like. The convex shape of the spectrum could be a result of an outburst of a flaring flat-spectrum source as well as a genuine GPS source. Additionally, five sources had a convex spectrum but high variability ($\mathrm{Var}_{\Delta S,MAX} > 3$) and the rest had steep ($\alpha_{above} < -0.5$) or flat ($\alpha_{below} < 0.5$) spectrum. For the parameters for each source type, see Table 1.

These results imply that the GPS galaxy samples have more genuine GPS sources than the quasar samples but yet a remarkable share of them have been misclassified. and with the current data sets cannot be classified as GPS sources. The variability of the galaxy-type GPS sources seems to be lower than that of the quasar-type GPS sources.

Table 1: Average parameters for different classes of sources in the second sample.

Proposed Class	N Sources	z	ν_{peak} GHz	α_{below}	α_{above}	$\mathrm{Var}_{\Delta S,MAX}$
gps	29	0.59	2.77	+0.91	-0.88	1.21
n	28	0.40	1.53	+0.78	-0.91	0.52
s	11	0.37	0.36	-	-0.84	0.78
f	9	0.95	1.69	+0.36	-0.44	1.30
f/s	14	0.78	0.32	-	-0.93	0.89
c	5	0.42	2.16	+1.15	-0.95	3.34
all	96	0.58	1.65	+0.86	-0.86	1.04

gps = Gigahertz-peaked spectrum

n = Not enough data for GPS identification

s = Steep spectrum

f = Flat spectrum

f/s = Flat at low freq., steep at high freq.

c = Convex (and variable) spectrum

4 Discussion and conclusions

Our studies show that among the GPS sources presented in the literature, there is a remarkable share of sources that cannot be classified as GPS sources when taking a closer look. A few simultaneous multifrequency observations in a year or two are not enough to reveal the variability behaviour of a source, and thus it is hard to distinguish the genuine GPS sources from sources with inverted spectrum during the flares as can be seen in Fig. 1.

When comparing the results of the galaxies and the quasars, one must bear in mind the heavy selection effect of the samples. The quasar sample was selected from the Metsähovi monitoring sample which has been monitored over 25 years. The galaxy sample, however, was gathered from the GPS literature and included both weak or seldomly observed sources and more frequently monitored sources, with a history of dozens of years of observations. The Metsähovi monitoring sources have originally been selected mostly because of their variability behaviour, and thus it is natural that the variability in this group of sources is high. A notable proportion of the galaxies had only a few detections and there is no sence in discussing their variability behaviour or long-term spectral characteristics based on the current data sets. Forbearing monitoring as well as simultaneous multifrequency observations are needed to distinguish the variable flat-spectrum sources from the genuine GPS sources.

For the Planck mission these results implicate a complicated situation. Instead of predictable, invariable GPS sources there are also sources with high-frequency flares that may or may not be detectable by Planck. Monitoring and modelling the variability of the GPS

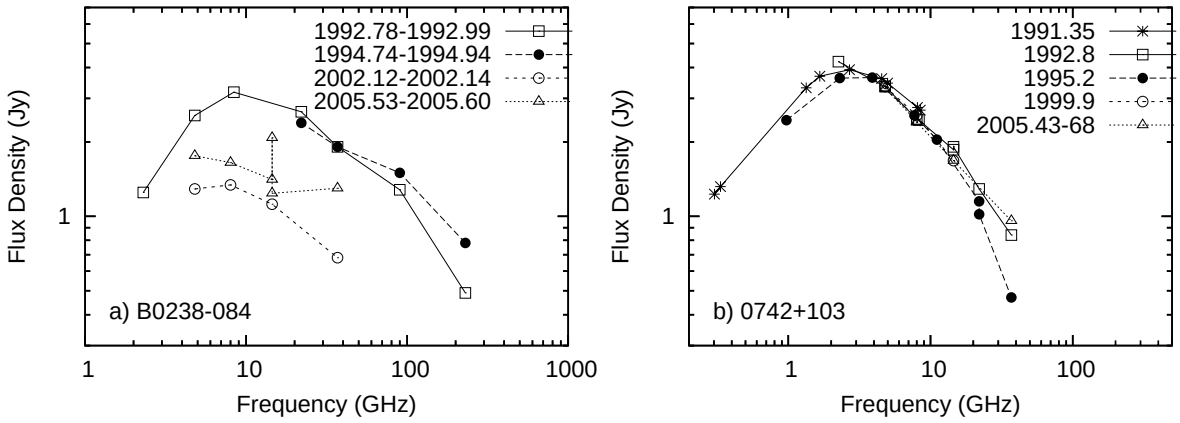

Figure 1: Semisimultanous spectra of a) B0238-084 and b) B0742+103. With the first two spectra, both sources could be classified as invariable GPS sources but longer monitoring reveals the difference in their behaviour.

sources will help us to make educated guesses of the number and the brightness of the foreground sources.

Acknowledgements. The authors made use of the database CATS (Verkhodanov et al. 1997) of the Special Astrophysical Observatory. UMRAO is supported in part by funds from the NSF and by funds from the University of Michigan Department of Astronomy.

References

Murgia, M., Fanti, C., Fanti, R. et al., *A&A*, 1999, **345**, 769
Mutel, R. L. and Phillips, R. B., *IAUS*, 1988, **129**, 73 Torniainen, I., Tornikoski, M., Teräsranta, H., Aller, M.F., Aller, H.D., *A&A*, 2005, **435**, 839.
Verkhodanov O.V., Trushkin S.A., Andernach H., Chernenkov V.N., *ASP Conference Series*, 1997, **125**, 322.

Long Term Radio Monitoring – Why Do We Need It?

M. Tornikoski [1)] , A. Lähteenmäki [1)] , E. Valtaoja [2)] , T. Hovatta [1)] , E. Nieppola [1,2)] ,
I. Torniainen [1)], M. Kotiranta [1)] , S. Trushkin [3)]

[1)] Metsähovi Radio Observatory, Metsähovintie 114, FI-02540 Kylmälä, Finland
[2)] Tuorla Observatory, Väisäläntie 20, FI-21500 Piikkiö, Finland
[3)] Special Astrophysical Observatory RAS Nizhnij Arkhyz, Karachaevo-Cherkesia, 369167, Russia

Abstract

Our group has studied the long term radio variability of Active Galactic Nuclei (AGNs) for more than 25 years. Our current source list for monitoring consists of more than 80 objects. Additionally, we have made few-epoch multifrequency observations of large source samples. In this paper we show that even though they are very useful for determining the instantaneous continuum spectrum and for studying the general properties of large source samples, few-epoch observations or even short term monitoring does not suffice for determining the true variability behaviour of most radio-loud AGNs. We also show that, for studying the overall variability, long term monitoring is much more important than dense sampling.

Introduction

The Metsähovi team has been active in the field of continuum monitoring of blazars since 1980 (Salonen et al. 1987; Teräsranta et al. 1992, 1998, 2004, 2005). The main observing frequencies have been 22 and 37 GHz, and some observations have been made using the 12 and 86 GHz frequency bands. Additionally, we have 15 years of 90 & 230 GHz monitoring data for near-equatorial sources from the SEST telescope (Tornikoski et al. 1996).

Our group has used the monitoring data for various purposes: for studying the long term multifrequency behaviour of individual sources (e.g., Rantakyrö et al. 2003; Lindfors et al. 2006), for studying individual flares in individual sources (e.g., Ogle et al. 2005; Pian et al. 2006), and for studying the multifrequency long term behaviour of larger source samples (e.g., Tornikoski et al. 2001; Torniainen et al. 2005).

In addition to the long term monitoring of a sample of blazars our group has invested time and effort in observing various new AGN source samples at high radio frequencies (Nieppola et al. 2006; Torniainen et al. 2006).

Planck pre-launch studies

Our team is a consortium member in European Space Agency's Planck satellite project. The main goal of Planck – to be launched in 2008 – will be to study the anisotropies of the Cosmic Microwave Background (CMB) by using nine frequency bands operating at high radio frequencies, between 30 and 857 GHz. To do so, the satellite will measure the whole sky twice. This means that it will also observe all sources emitting at radio frequencies, also the ones in front of the CMB signal. In order to get accurate CMB maps, these foreground radio sources

must be separated from the CMB radiation and its tiny irregularities. For this we need to know the number and brightness of the foreground sources.

Already our earlier studies (Tornikoski et al. 2000, 2001), have revealed that many AGNs that have been excluded from high-frequency radio observing campaigns because they have been *assumed* to be too faint and uninteresting in the millimetre-domain can, in fact, at least occasionally be very bright. Because of very limited telescope time available in the millimetre-domain, many source samples for high-frequency studies have been formed based on only one- to few-epoch observations at lower frequencies (typically 5 GHz or below). Usually this means selecting objects that are expected to be bright based on their historical low-frequency data. Thus there is a large number of objects for which we possess no true knowledge of their high-frequency fluxes and variability.

In order to get a better understanding of the millimetre-behaviour of the possible Planck foreground sources – their estimated number, fluxes, characteristic variability behaviour, etc. – we have used the Metsähovi radio telescope for making pre-launch observations of large new source samples at 37 GHz. These include a sample of gigahertz-peaked spectrum (GPS) sources and candidates (Torniainen et al. 2006, and these proceedings) and a complete sample of BL Lacertae Objects (BLOs) (Nieppola et al. 2006, and these proceedings). We have also used the RATAN-600 telescope to obtain simultaneous 1-22 GHz data at several epochs to complement our 37 GHz data and to obtain true continuum spectra for these sources.

A few years of data. How much do we really know?

Some examples of sources from our multifrequency observing campaigns are presented in Fig. 1 (a, b).

In Fig. 1a) we have plotted the multi-epoch, multifrequency data for TEX1040+244. This source is included in our complete sample of BL Lacertae Objects (Nieppola et al. 2006). The low-frequency data plotted using black symbols are historical data from the literature and show the source in a relatively faint state. The 37 GHz data are from our Metsähovi observing project that started in 2001. Due to the variability and brightness, this source was also included in our RATAN-600 followup observations (the coloured symbols from various epochs between November 2003 and February 2005).

In Fig. 1b) we have plotted the data for S20109+227. Much more data were available for this source from the literature, including a historical RATAN-600 spectrum from 1997 (Kovalev et al. 1999) (grey symbols).

For both of the sources featured here it is obvious that prominent variability occurs over a wide frequency range. It is important to note, however, that the 2003-2005 data sets show less variability compared to each other than compared to the historical fluxes. This is even more pronounced for S20109+227, for which the 2003-2005 spectra remain relatively flat but where the 1997 spectrum is highly inverted.

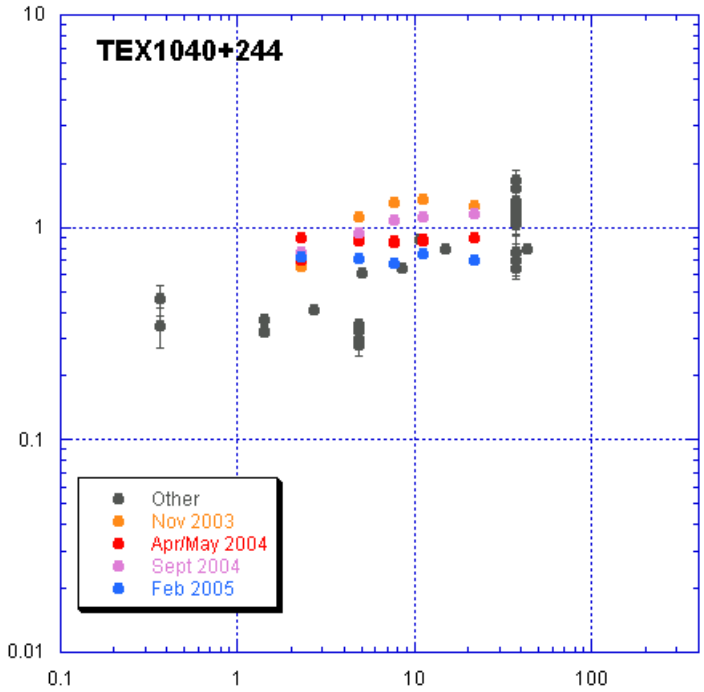

Fig 1a). Multi-epoch, multifrequency data for TEX1040+244. The coloured symbols are simultaneous 1-22 GHz data from RATAN-600, each colour being from different observing epoch as indicated in the legend. The black symbols are non-simultaneous data from the literature or from our group's observations in Metsähovi.

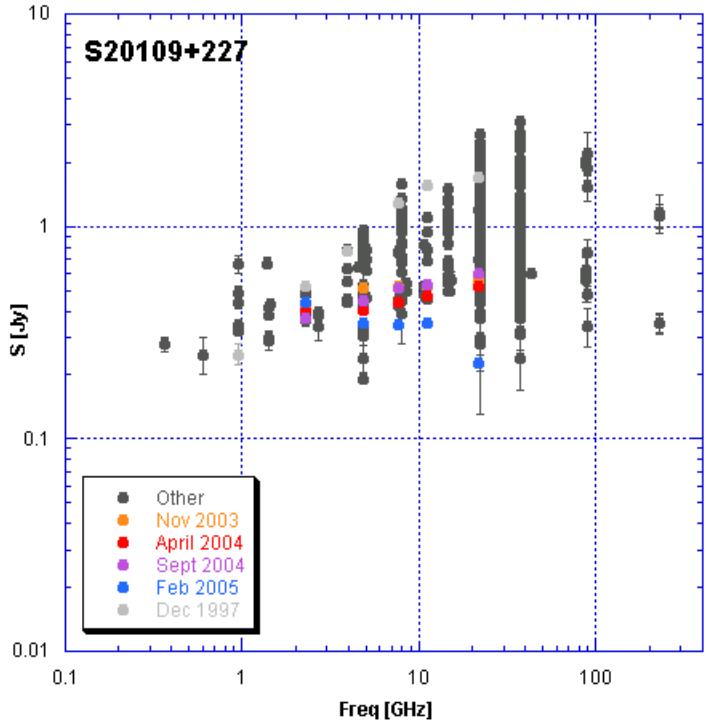

Fig 1b). Multi-epoch, multifrequency data for S20109+227. The coloured symbols are simultaneous 1-22 GHz data from RATAN-600, each colour being from different observing epoch as indicated in the legend. The grey symbols are earlier RATAN-600 data from 1997 (Kovalev et al. 1999). The black symbols are non-simultaneous data from the literature or from our group's observations in Metsähovi.

When we inspect the data obtained during our multifrequency observations and compare these data with historical data points from the literature, we can conclude the following:

1) Many of the sources in our samples have very different flux levels during our observations when compared to the historical values.
2) During our campaign of multifrequency (Metsähovi + RATAN-600) observations over the period of ca. 1.5 years many sources neither reach their historical minima nor maxima.
3) The shape of the continuum spectra can vary considerably between the historical data (including the 1997 data published in Kovalev et al. 1999) and our data sets.
4) Even though our relatively short set of RATAN-600 spectra also show variability, no extremely drastic changes are seen between the data sets obtained during the 1.5 years of observations.

The results suggest that for variable sources, a few years of observations is not sufficient to reveal their true variability behaviour. With much longer data sets we see the actual flux minima and maxima, as well as some dramatic changes in the shape of the continuum spectrum. These findings are similar to those of Torniainen et al. (2005, 2006, and these proceedings).

The importance of the longer term data taking can be easily verified by studying the flux curves of the sources from our long term monitoring project. In Fig.2 (a, b) we have plotted some examples of the densely monitored sources from our monitoring project. Even though these two sources exhibit very different variability behaviour in terms of the flare occurance during the observing period of over 25 years, as well as of the flare timescales, we can see that by randomly extracting any 2-4 year data stream from these flux curves we get data sets that would be hard to identify as being from one single source. Some of them would show almost violent variabilty whereas some others would show relatively constant or only moderately variable flux levels.

When comparing the flux curves from our current data set of over 25 years to the 10-year data published for the same sources in Teräsranta et al. (1998) , we can easily see that even the 10-year data sets are relatively short: even for many of the bright and variable sources only one prominent flare occurs in the 10-year data stream.

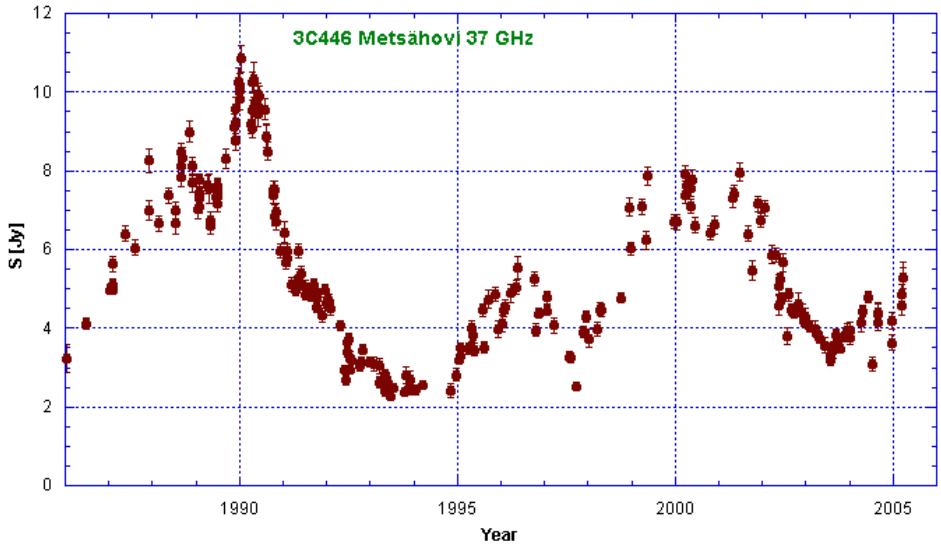

Figure 2a). The Metsähovi 37 GHz flux curve for 3C446.

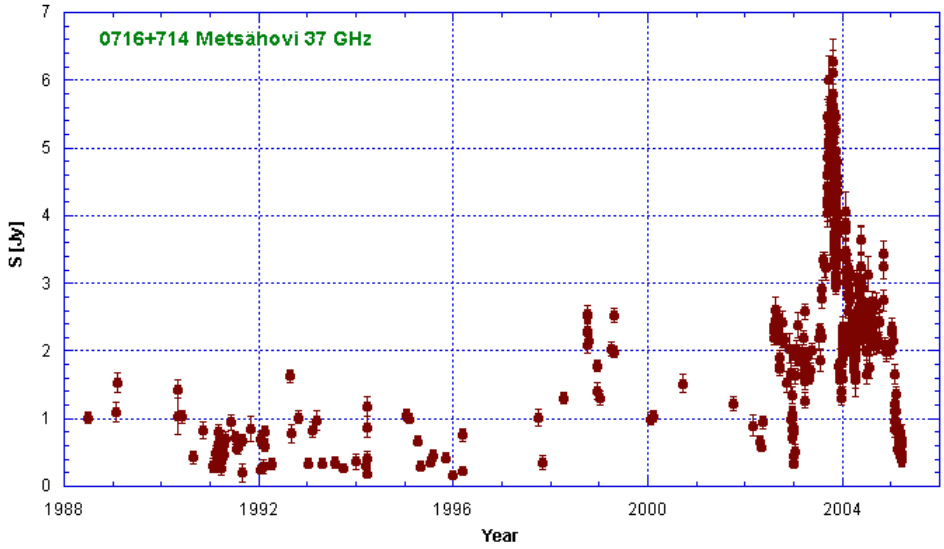

Figure 2b). The Metsähovi 37 GHz flux curve for 0716+714.

Variability statistics

In order to better understand the long term radio variability, we used our sample of the best-monitored (= long and dense data sets) sources to study the typical variability behaviour of blazars.

In Hovatta et al. (these proceedings and in preparation for the A&A) we studied the variability behaviour from our 25 years of observations of altogether 80 sources, including high polarization quasars, low polarization quasars, BL Lacertae Objects and some radio galaxies, in order to find out the typical variability timescales. We found that the typical peak-to-peak timescales at the Metsähovi observing frequencies are of the order of seven years. Mathematical analysis methods as well as a visual inspection of the light curves reveal that also shorter timescales are present, but the general trend is that the time between two large flares is very long, several years.

In Tornikoski et al. (2000) we used a simple method (based on the number of data points taken during each activity state) for estimating the times spent in various activity states. We found out that among the sources in our SEST sample, one is less likely to observe a source in a flaring state than in a quiescent or intermediate state. We wanted to repeat this handling by using a more reliable method for our dense and long Metsähovi database of 80 sources. By using the information of the all-time flux minima and maxima from 25 years of observations, we divided the flux curves into three equal parts and labelled them the “quiescent”, “intermediate” and “active” states. We randomly chose several target epochs and used interpolated flux curves in order to define the activity state during that particular epoch for each source in our sample. We found out that at 37 GHz the distribution among the various states from the several randomly chosen epochs is on average: 11% in the active state, 38% in the intermediate state, and 51% in the quiescent state. This means that 9 times out of 10 we are likely to see the source in a quiescent or in an intermediate state!

We also wanted to see how much the sampling density affects our results. For our monitoring sample, the average observing interval is 35 days at 22 GHz and 51 days at 37 GHz, with the most densely sampled sources having been observed 2-4 times every month and even much more

densely during some intensive observing campaigns (prominent outbursts, multifrequency campaigns, etc.). Using our real data, we produced data streams of less densely sampled data (varying our sampling from 3 to 6 samples per year), distributed over the year as evenly as possible, and we compared these modified flux curves with the original ones. Even though some peak events of rapid flares were now excluded from the artificial flux curves, the general trends were still easily seen in the less densely sampled data streams. Typically data points from both the rise and decay stages of the flares were still included, except for the most rapid flares. We can conclude that in order to study the general trends of the variability behaviour (peak-to-peak fluxes and typical flare timescales, as opposed to the study of the very detailed flare characteristics or the intra-day variability etc.), long term monitoring is much more important than very dense sampling. These findings are also confirmed by a more accurate study of the actual flare timescales (Hovatta et al., in preparation for the A&A). Ideally, one would naturally want to combine long term monitoring with sufficiently dense sampling.

Discussion

The fact that the most interesting radio events in AGNs occur relatively rarely, has several important implications.

First of all, in order to fully understand the variability behaviour, long term monitoring is crucial and indeed even more important than very dense sampling. Unfortunately it is often difficult to obtain telescope time for repeated observations and persistent, long-term monitoring especially if the first few data sets do not produce results that can convince the telescope programme committees to continue the project. This emphasizes the value of the few dedicated monitoring telescopes.

It is important to understand that the few-epoch / short-term observing campaigns – even though valuable for other purposes – may offer results that easily lead into incorrect interpretations of the source behaviour, either on individual sources or sometimes even on large source samples. These may include incorrect interpretations of the continuum spectrum, variability, detectability or even their possible contribution to the CMB foreground. It may also lead into incorrect classification of objects, as clearly pointed out in Torniainen et al. (2005, 2006, and these proceedings), and thus into misinterpretation of source types or subtypes, and ultimately to incorrect theoretical models. Additionally, potentially interesting objects are often excluded from subsequent studies if they happen to be in a relatively faint state during the short observing campaigns. This is especially true for the millimetre- and submillimetre domain, where telescope time is more difficult to obtain and observations of sources that are “known” to be faint are often considered a waste of valuable observing time.

Secondly, based on the relatively low probability of detecting a source in a flaring state, it is clear that many multifrequency observing campaigs that are planned well in advance are likely to catch a source in a fainter state. Naturally, sometimes very useful results can be drawn also from observations made in a faint state (e.g., Türler et al. 2006), or the source can by chance exhibit unforeseen activity behaviour (e.g., Ostorero et al. 2006; Villata et al. 2006).

In order to better understand the activity behaviour of the sources in the Metsähovi sample (both in the “classical” monitoring sample as well as the various recently added larger source samples) our team is attacking the variability problem from various sides. We are studying the long term variability characteristics as well as the individual flares of our monitoring sources by using many different methods ranging from statistical and other mathematical methods to flare

decomposition & analysis. Our ultimate goal is both to be able to predict radio flares in these sources, based on the earlier multifrequency flux history and advanced analysis methods, as well as to more accurately understand the physics of the radio shocks.

Conclusions

We have studied the long term variability of AGNs in Metsähovi for more than 25 years, mainly using the 22 GHz and 37 GHz frequency bands. Additionally, we have made few-epoch observations of several large source samples (e.g., GPS sources and candidates, and a complete sample of BL Lacertae Objects), complementing our Metsähovi data with the simultaneous 1-22 GHz data from the RATAN-600.

We have found out that for the bright and active radio-loud AGNs in our monitoring sample, prominent radio flares occur relatively rarely. The average timescales between large flares are on the order of seven years. We have also shown that the sources in our sample spend more time in the quiescent or intermediate state than in the active state – the chance to randomly observe a source in a flaring state at 37 GHz is one out of ten! On the other hand, even in the millimetre domain the typical timescales of the flares are relatively long, and thus very dense monitoring is needed only for studying the details of the flares or very short-term changes like the intra-day variability.

We conclude that only long-term monitoring can reveal the true variability behaviour of most radio-loud AGNs. This seems to be true also for the more sparsely observed sources, for which incorrect interpretations have often been made based on too few epochs of data.

References

Lindfors, E. et al. A&A 456, 895, 2006.
Nieppola, E. et al., AJ, in press, 2006.
Kovalev, Y. et al., A&AS 139, 545, 1999.
Ogle, P. M. et al., ApJ 618, 1390, 2005.
Ostorero, L. et al., A&A 451, 797, 2006.
Pian, E. et al., A&A 449, L21, 2006.
Rantakyrö, F. et al., A&A 405, 473, 2003.
Salonen, E. et al., A&AS 70, 409, 1987.
Teräsranta, H. et al., A&AS 94, 121, 1992.
Teräsranta, H. et al., A&AS 132, 305, 1998.
Teräsranta, H. et al., A&A 427, 769, 2004.
Teräsranta, H. et al., A&A 440, 409, 2005.
Torniainen, I. et al., A&A 435, 839, 2005.
Torniainen, I. et al., A&A, submitted, 2006.
Tornikoski, M. et al., A&AS 116, 157, 1996.
Tornikoski, M. et al., AJ 120, 2278, 2000.
Tornikoski, M. et al., AJ 121, 1306, 2001.
Türler, M. et al., A&A 451, L1, 2006
Villata, M. et al., A&A 453, 857, 2006.

Quasar Host Galaxies in the FORS Deep Field

Carolin Villforth
Jochen Heidt
ZAH, Landessternwarte Heidelberg, Germany
Kari Nilsson
Tuorla Observatory, Finland

October 24, 2006

Abstract

The evolution of quasar host galaxies is still hardly studied at high redshifts ($z > 2$), although this is a very interesting redshift range as the quasar activity peaks at z≈2-3. We have studied the evolution of quasar host galaxies at high redshifts up to $z \approx 3.4$. Eight quasars from the FORS Deep Field were analyzed with redshifts lying between z=0.87 and z=3.37. We used the 2D-fitting program kimage to resolve the hostgalaxies. The quasars were studied in eight filters from the near UV to the near IR. Using the magnitudes in different filters we investigated the presumed galaxy type and the mass of the central black hole of the resolved galaxies. For four quasars between z=0.87 and z=2.75 their hostgalaxies could be resolved. The absolute k-corrected magnitudes in the I-band are between M_I=-22.22 and M_I=-26.80. One host galaxy was unambiguously identified as a disk galaxy, for the other host galaxies such a clear identification was not possible. The upper limits for the masses of the central black holes are $\sim 10^7 - 10^8 M_\odot$. Comparing our results with those of other authors we found that host galaxies of radio-loud and radio-quiet evolve differently; if corrected for passive evolution the absolute magnitude of host galaxies of radio-loud quasars stays constant up to a redshift of $z \approx 3$ whereas the absolute magnitude of host galaxies of radio-quiet quasars decreases distinctly at redshifts higher than $z \approx 2$.

1 Introduction

The peak of the quasar activity lies at z≈2-3 (see Nandra et al. [2005]). This is also the redshift range at which the brightness (k-corrected) of quasar host galaxies seems to decrease (e.g. Falomo et al. [2005]), though this decrease is poorly constrained due to small samples at high redshifts. Although the formation and evolution of nuclear activity is not yet understood it seems to be clear that there is a strong link between the evolution of galaxies and nuclear activity. After the observational confirmation of supermassive black holes in nearby early-type galaxies, correlations between the properties of the host galaxy and its central black hole were found (e.g. Novak et al. [2006]). This affirmed the assumption that the evolution of early-type galaxies and the central black hole, and thus nuclear activity, are linked.

The evolution of the host galaxies of quasars has been studied over a wide redshift range from very low redshifts (e.g. Dunlop et al. [2003]; Percival et al. [2001]) up to very high redshifts of $z \sim 3$ (e.g. Ridgway et al. [2001]; Falomo et al. [2005];

Falomo et al. [2004]; Jahnke et al. [2004]). It was established that quasars mostly reside in luminous massive early-type galaxies. The k-corrected luminosity of the host galaxies increases with redshift. The host galaxies of radio-quiet quasars seem less luminous than the host galaxies of radio-loud quasars (e.g. Kukula et al. [2001]). Quasar host galaxies at high redshifts of z=2∼3 have not been studied elaborately so far, as investigation of quasar host galaxies at high redshifts requires not only excellent resolution but also very deep imaging to guarantee a signal-to-noise high enough to be able to detect the host galaxies, which are mostly far less luminous than the core. Thus the evolution of the host galaxies at high redshifts is still poorly investigated. The investigation of quasars at high redshift is a difficult task. At very high redshifts the extension of the host galaxy merely exceeds the PSF, thus studies of high-redshift quasars mostly used the HST (e.g. Kukula et al. [2001]; Jahnke et al. [2004]; Ridgway et al. [2001]). Jahnke et al. ([2004]) found rest-frame absolute magnitudes at 200nm of $-20.0 < M_{200nm} < -22.2 mag$, but did not study morphological properties. Kukula et al. ([2001]) found absolute V-band magnitudes around $-22 < M_V < -24 mag$, early-type morphologies and different evolution for RQQ and RLQ host galaxies. For his samples, host galaxies of RQQ are fainter than those of RLQ with a growing gap towards higher redshifts. Adaptive optics observations begin to play an important role in the exploration of quasar host galaxies(e.g. Falomo et al. [2005]). The host galaxy with the highest redshift using AO observations detected so far had z=2.93. Falomo et al. ([2005]) found an early-type galaxy with r_e=7kpc and $M_K \sim -27$.

Apart from higher redshifts another part of the research of quasar host galaxies is still unsettled. Most imaging of quasars was done in one or two filters, the determination of host galaxy type was based solely on their surface brightness distribution. Investigations of stellar populations, star formation rates or age of the host galaxy are difficult or even impossible using magnitudes in only one or two filters. Recently a spectroscopic study of quasar host galaxies at low redshift (z∼0.3) was carried out by Letawe et al. [2006]. Most galaxies were found to have Sc-like populations, showing large amounts of ionized gas and signs of interaction, which is somehow contradictory to the fact, that luminous quasars mostly reside in massive early-type galaxies. Canalizo & Stockton ([2001]) analyzed a sample of low-redshift quasars (z⩽0.4) spectroscopically using LIRS and Keck II. They found tidal interaction-induced starburst in almost all of their objects. For 5/9 sources they found star-forming regions in the center which is consistent with merger-induced starbursts. They found clues, that central starbursts and QSO activity were triggered simultaneously. However, these studies are only possible for extended host galaxies at very low redshift, otherwise it is not possible to separate the spectrum of the host galaxy and the spectrum of the active nucleus sufficiently.

In this work we will analyze eight quasars from the FORS Deep Field (FDF). Due to extremely long exposure times (up to 44400s in U), the images are extremely deep with 50% completeness limits up to 27.7 in the B-band. Additionally the seeing is excellent, with the best seeing being 0.53" in the I-band. The field was observed in a wide wavelength range from near UV (U) to near IR (J and Ks). Thus we were able to analyze our objects in 8 broadband filters from near UV to near IR allowing multiband analysis of the host galaxy from rest-frame UV to restframe optical. This gives us the possibility to study the probable galaxy type and mass of central black hole of the host galaxies.

All magnitudes are given in the Vega-system. The cosmology used is
$H_0 = 70 km/s/Mpc$, $\Omega_\Lambda = 0.7$, $\Omega_m = 0.3$, unless otherwise stated.

Table 1: The QSO-Sample

FDF-ID	z	RA	DEC	m_I	type
FDF0809	0.8650	01:05:50.3	-25:44:48	21.4	QSOI
FDF1837	2.2540	01:05:54.2	-25:46:41	22.9	QSOI
FDF2229	2.1560	01:05:55.7	-25:47:22	20.8	QSOI
FDF2633	3.0780	01:05:57.3	-25:44:57	22.8	QSOI
FDF4683	3.3650	01:06:04.4	-25:46:51	18.6	QSOI
FDF5962	1.7480	01:06:09.0	-25:42:56	21.9	QSOI
FDF6007	2.7515	01:06:09.2	-25:43:26	24.1	QSOII
FDF6233	2.3215	01:06:10.0	-25:43:42	23.9	BAL

2 The QSO-Sample

The QSO-sample consists of eight quasars in the FDF, the redshifts of the objects are between z=0.87 and z=3.37. Except FDF4683, all quasars are radio-quiet. They were identified spectroscopically by Noll et al. [2004]. The basic properties of the quasars can be found in Table 1.

The FDF was carefully selected to contain no stars brighter than 18th magnitude but to contain a high-redshift-quasar (FDF4683 at z=3.37). The field is about 7'x7' and contains about 9000 objects, for about 350 of these objects spectroscopy was performed.

Observations were carried out using the VLT (UBgRI and spectroscopy), the NTT (J and Ks) and the HST (F814W). A detailed description of field selection and photometry can be found in Heidt et al. [2003], a description of the spectroscopic sample and observations can be found in Noll et al. [2004].

Observations were made from august 1999 to august 2000, the conditions were mostly photometric. Very good seeing could be achieved, lying between 0.53" for the I-band and 0.97" for the U-band, the seeing for the NIR-data was slightly worse, with values of about 1.2". Due to extremely long exposures ranging from about 6 to up to 12 hours in the optical and UV-bands, the images are extremely deep with 50%-completeness limits of 25.64 to 27.69 in the optical bands. The NIR are far less deep due to notedly shorter exposure times of 4800s. The HST-data have the best resolution, however the exposure time is quite short being 2400s.

3 Data Analysis

The data were analyzed using a 2D-fitting routine based on a Levenberg-Marquardt-loop (see Nilsson et al. [1999]). To resolve the host galaxy, three different fits were done for each object in each filter. First, a point-source was fitted to the quasar to determine the center coordinates of the objects and as a comparison for the decision if the host galaxy is resolved or not. This fit had three free parameters: the magnitude of the point source and the x- and y-coordinate. Maintaining the determined center coordinates a core+galaxy-model was fitted to the object with the galaxy being either a disk with an exponential light profile or a bulge with a de Vaucoleurs profile. The galaxy models were folded with the PSF. This fit has three free parameters: the magnitude of the central point source and the magnitude and effective radius of the galaxy. For the object with the lowest redshift (FDF0809 at z=0.87) an additional fit with five free pa-

rameters (magnitude of central point source, magnitude, effective radius, ellipticity and position angle of the galaxy) was carried out since its host galaxy was well resolved.

The construction of a PSF is a very critical point, as for such high redshifts and thus minor extension of the host galaxy, the PSF needs to be exactly known. This was very difficult here, since most of the QSOs were brighter than the brightest stars in the FDF (which was by definition selected to have no bright stars). Thus the PSF was constructed by a combination of as many as possible well selected stars.

For the HST-data it was also difficult to extract a PSF, as it shows strong variations over the field. Thus much effort was made to find a good PSF for each quasar. In the end it was decided to use a PSF by stacking all suitable stars in the field.

The host galaxy is resolved if the χ^2 for one of the core+galaxy-fits is significantly better than the core-fit. For marginal detections, error simulations were performed to decide if the object is resolved or not.

To do so, the object is simulated using the results of the fits, the model was folded with the used PSF, and noise was added. Afterwards, the simulated objects were fitted. Approximately 20-50 simulations are done for each object. The criteria for the object being resolved or not is: $5*\sigma_{r_{e,simulated}} < r_{e,fits}$, with $\sigma_{r_{e,simulated}}$ being the standard deviation of the effective radius from the simulations and $r_{e,fits}$ being the measured effective radius. This has to be the case in at least one filter for the particular object.

4 Results

For four out of the eight quasars (FDF0809, FDF1837, FDF2229, FDF6007) the host galaxy could be resolved. FDF0809 could be resolved in all filters, the others were resolved in all optical bands. Apart from FDF6007, where no fit was possible in U due to the faintness of the object in this band. Only one object (FDF0809) was resolved in the HST-band F814W. Error simulations yielded the following results: FDF0809 is clearly resolved, FDF1837 and FDF2229 are marginally resolved and FDF6007 is well resolved. The absolute k-corrected magnitudes of the resolved host galaxies can be found in Table 2. We found effective radii, exemplary in the I-band, between 0.9 and 5.3 kpc, with a mean of 2.3±1.7kpc. The absolute magnitudes of the resolved objects lie in the following ranges in the different filters: -21.02 to -28.46 (U), -20.02 to -28.16 (B), -21.32 to -28.46 (g), -22.02 to -28.10 in R, -22.22 to -26.80 in I and -22.26 to -23.34 in the HST-band F814W. In the NIR-bands J and Ks it was only possible to resolve the low redshift (z=0.8650) source FDF0809.

Concerning their morphology, a disk type galaxy was distinctly preferred for object FDF0809 (clearly better χ^2) in the filters B, I, J and Ks. As B and I are the filters with the best seeing, this is a clear argument for disk morphology. For FDF1837 and FDF2229, a disk type galaxy is slightly preferred for the filters R and I, though, χ^2 shows only small differences for the different models. For FDF6007 a disk-dominated and a bulge dominated host galaxy can equally well be fitted.

5 Discussion

5.1 Comparison with other authors

In Figure 1 we compare our results in the I-band to those of Jahnke et al. [2004]; Falomo et al. [2004]; Falomo et al. [2005]; Percival et al. [2001]; Dunlop et al. [2003];

Table 2: Absolute magnitudes for the resolved host galaxies, k-corrected (Bicker et al. [2004]). Values for FDF0809 are from the fit with variable ellipticity and PA

object	M_U	M_B	M_g	M_R	M_I	M_{F814W}	M_J	M_{Ks}
FDF0809 [disk]	-21.02	-20.02	-21.32	-22.02	-22.22	-22.26	-22.62	-23.62
FDF0809 [bulge]	-24.12	-22.52	-22.52	-23.12	-23.12	-23.34	-22.62	-23.32
FDF1837 [disk]	-21.59	-20.29	-22.29	-23.09	-23.89	–	–	–
FDF1837 [bulge]	-27.19	-25.89	-27.69	-26.09	-26.29	–	–	–
FDF2229 [disk]	-23.46	-22.26	-23.86	-24.16	-24.66	–	–	–
FDF2229 [bulge]	-28.46	-28.16	-28.46	-27.76	-26.76	–	–	–
FDF6007 [disk]	–	-21.40	-21.40	-22.70	-22.90	-22.95	–	–
FDF6007 [bulge]	–	-27.50	-27.10	-28.10	-26.80	–	–	–

Kukula et al. [2001]; Ridgway et al. [2001]. The top panel shows the k-corrected, the bottom panel the k+e-corrected magnitudes. K-corrections are from Bicker et al. [2004], color-corrections are from Poggianti [1997] (these were used to convert magnitudes from different filters to I-band). In addition, the values for M* galaxies of type E and Sb are displayed (data based on Bruzual & Charlot [1993]). For the evolutionary correction the cosmology had to be changed to $H_0 = 70km/s/Mpc, \Omega_0 = 0.1$ as no other values for the e-correction were available up to this redshift, they are from Bicker et al. [2004]. For this plot, the values for M* are also from Bicker et al. [2004]. Evolution correction assumes exponentially seceding star formation rate with an e-folding time of 1Gyr for a spheroidal galaxy (type E). For spirals a star formation rate linearly proportional to the gas-to -total mass ratio with characteristic timescales from 4Gyr for Sa through $t > 15Gyr$ for Sd is assumed.

In Figure 1 (k+e-corrected) a slow but distinct decrease of the absolute magnitude beyond z=2 is visible. Thus it seems reasonable that QSO host galaxies evolve considerably in this redshift range.

In Figure 2 we show the same diagram as in Figure 1 (lower panel) just using the results for elliptical host galaxies, this time separated by RLQ and RQQ averaged in separate bins over look-back time. It is obvious, that host galaxies of radio-loud and radio-quiet quasars evolve differently. The host galaxies of radio-quiet quasars are fainter on average than RLQ hosts. In addition, their luminosity decreases considerably compared to RLQ hosts within 2Gyr. This suggests that host galaxies of radio-loud quasars formed earlier, whereas host galaxies of radio-quiet quasars seem to have formed in the redshift range between $z \approx 2.5 - 3$.

Note, however, that the samples used in the interesting high-z-range are still very small and our conclusions somewhat uncertain. Host galaxies can typically only be detected if they are not more than 2.5mag fainter than the AGN. Since only bright RLQ were studied so far (due to a lack of available faint RLQ), figures 1 and 2 can severely be biased.

5.2 Simulation of spectra

Since we have deep spectra of our QSO from the FDF, we compared the results of our fits to them. The method is as follows: the fitting program produces model images. These images were used to simulate spectroscopy with a 1" slit (corresponding to the slit width used for the FDF-spectra). This was done for all objects in the I-band and for FDF0809 in the B-band. We used a QSO-template by J.R. Walsh based on Francis et al. [1991] and an elliptical galaxy and a spiral Sb galaxy template from Kinney et al. [1996]. The template spectra had to be calibrated. This was done by folding

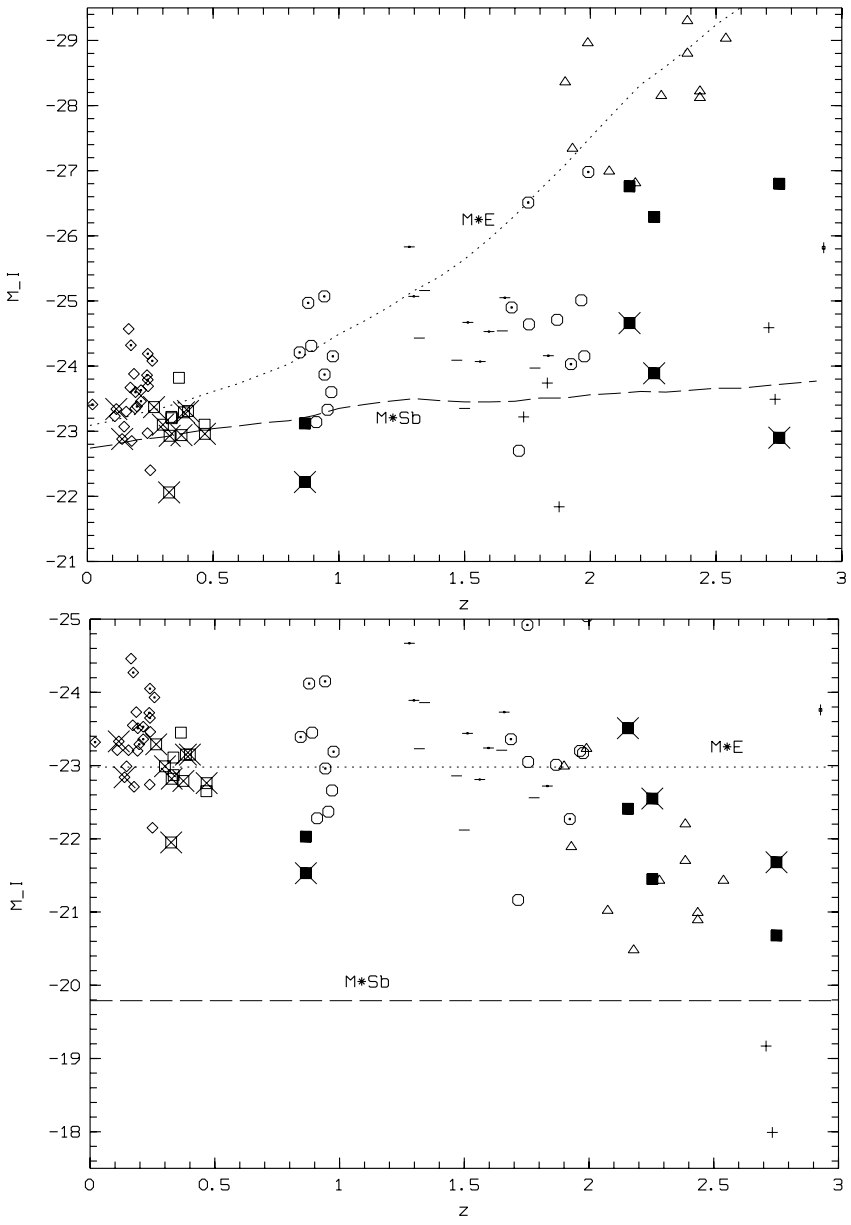

Figure 1: Comparison of the absolute magnitudes of quasar host galaxies in the I-band from different authors. Upper panel only k-corrected, lower panel k- and e-corrected. Data from this paper: filled squares (all are radio-quiet); other symbols: dotted symbols: hosts of RLQ, crossed symbols: disk type host galaxy.

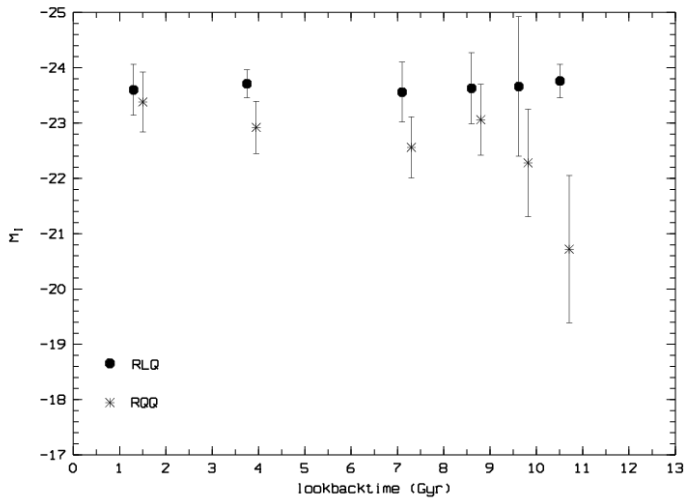

Figure 2: Evolution of elliptical quasar host galaxies of RLQ (dot) and RQQ (star) separately over look-back time.

Table 3: Mass of the central black hole (in $log(M_{BH}/M_{\odot})$ of the resolved galaxies for the different methods used: Gebhardt: G(B); Marconi & Hunt: MH(J); Bettoni et al.: B(R); McLure & Dunlop: MD(R).

object paper (filter) ->	G(B)	MH(J)	B(R)	MD(R)	average
0809	(8.48)	(7.39)	(8.39)	(8.29)	(8.1)
1837	6.76	–	7.35	7.35	7.2
2229	9.45	–	7.53	7.51	8.2
6007	7.27	–	7.45	7.44	7.4

the template spectra with the transmission curves of the filter and transformed to the restframe of the object. The spectrum was then scaled to flux 1 in this virtual filter. The calibrated spectra were weighted with the flux of the central point source and the host galaxy respectively. Finally the two weighted spectra were summed up and compared to the spectrum of the object. For FDF0809 a spiral galaxy is clearly favored over an elliptical galaxy, both for the I and the B-band (see Figure 3). For the other three objects simulation of spectra did not provide any useful results, neither an elliptical nor an disk type galaxy could be rejected.

5.3 Investigation of the mass of the central black hole

Evidence has been found that there are massive black holes in the centers of early-type galaxies. Due to high resolution data from the Hubble Space Telescope, it was possible to derive the mass of the central black holes for a number of nearby galaxies (see e.g. Kormendy & Gebhardt [2001]). Hence it was possible to derive relations between the mass of the central black hole and other properties of its hosting galaxy.

We estimated BH masses for our QSOs using the correlations provided by Novak

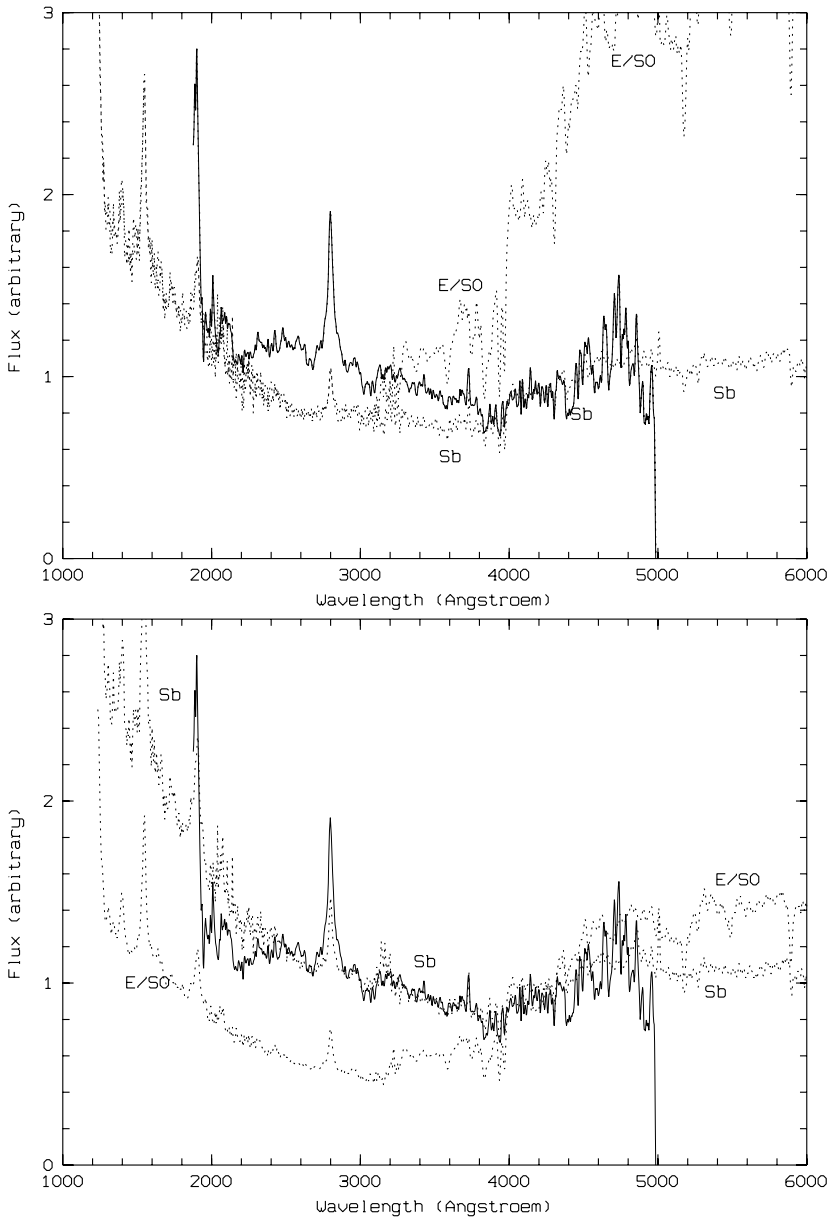

Figure 3: Simulation of the spectrum of FDF0809 in the I-band (lower panel) and B-band (upper panel). The solid line shows the measured spectrum in the restframe, the dashed lines show the simulated spectra marked with the model type of the galaxy template. The Sb-model is unambiguously preferred in both cases.

et al. [2006], Gebhardt et al. [2003], Marconi & Hunt [2003], Bettoni et al. [2003] and McLure & Dunlop [2001]. The results are shown in Table 3. Our results are clearly rendered by the fact that the relations were derived for local galaxies. We thus used the k+e-corrected galaxy luminosities. It is clear that we can derive only upper limits, since we do not know if and how galaxies and BHs evolve coeval.

On average our BH masses are between $\sim 10^7 - 10^8 M_\odot$.

The results for FDF0809 are only given for completeness, since the galaxy is a disk galaxy and the relations are only valid for early-type galaxies.

The values found using this method agree quite well with those of Ridgway et al. ([2001]), who found values from 0.29-2.19 $10^8 M_\odot$ for their z$\approx$ $1.8 - 2.7$ sample. Though, Ridgway et al. ([2001]) used another method to find out the mass of the central black hole, they used a correlation between the mass of the bulge and the mass of the central black hole. The mass of the black hole was determined using M/L-ratios corrected for passive evolution. Note that the cosmology used by Ridgway et al. ([2001]) is $H_0 = 50 km/s/Mpc, \Omega = 1$, whereas our cosmology is $H_0 = 70 km/s/Mpc, \Omega_0 = 0.1$. Values cannot be made consistent as corrections are only available for the used cosmology respectively.

6 Summary

In this work we presented a multiband (8 filters from UV to NIR) analysis of 8 high-redshift quasars (z=0.87-3.37). In four quasars between z=0.87 and z=2.76 the host galaxy could be resolved. For the resolved host galaxies we simulated spectra and derived upper limits for the BH masses of the QSOs.

To confirm the results for the morphology from the fits, we performed simulations of the spectra. This yielded excellent results for FDF0809, where a disk galaxy was clearly preferred over an early-type galaxy. For the other three resolved host galaxies our simulations do not favor one galaxy type over the other.

The mass of the central black hole was calculated using correlations between absolute magnitude of the host galaxy and the mass of central black hole calibrated with nearby spheroidal galaxies. As it is not clear whether these correlations are still valid for high-z objects, we used the k+e-corrected magnitudes. Thus our results are mere upper limits. The values found for the upper limits are $< 10^7 \sim 10^8 M_\odot$.

To constrain the evolution of quasar host galaxies we compared our results for the absolute k+e-corrected magnitude in the I-band to those of other authors transformed to the I-band. We found a distinct decrease at z$\sim$2-3. The host galaxies of RLQ clearly evolve differently than the host galaxies of RQQ. Up to z$\sim$2, the host galaxies of RQQ are just slightly fainter than those of RLQ. At higher redshifts, the host galaxies of RQQ show a distinct decrease in brightness of about factor 100 in only $\sim$1-2Gyr, whereas the brightness of RLQ hosts seems to be constant up to z=3. This would imply that the host galaxies of RQQ may have formed at redshift $z \sim 2 - 3$, whereas host galaxies of RLQ must have formed earlier. However, our results are based on small samples. In addition, selection effects may play a role.

To analyze QSO host galaxies at high-z very deep images with best resolution are required. Thus the use of AO at 8m-class telescopes will play an important role in the investigation of high redshift quasar host galaxies in the future. This will help to prove or disprove the present thesis on the evolution of quasar host galaxies. Auxiliary further exploration of the mass of the central black hole and properties of the galaxies like SFR

or stellar populations will help to understand triggering and evolution of quasars, their host galaxies and galaxies in general.

References

[2003] Bettoni, D., Falomo, R., Fasano, G., Govoni, F. 2003, A&A, 399, 869

[2004] Bicker, J., Fritze-v. Alvensleben, U., Möller, C.S., Fricke, K.J. 2004, A&A, 413, 37

[1993] Bruzual, A.G., & Charlot, S. 1993, ApJ, 405, 538

[2001] Canalizo, G., & Stockton, A. 2001, ApJ, 555, 719

[2003] Dunlop, J.S., McLure, R.J., Kukula, M.J., et al. 2003, MNRAS, 340, 1095

[2004] Falomo, R., Kotilainen, J.K., Pagani, C., Scarpa, R., Treves, A. 2004 ApJ, 604, 495

[2005] Falomo, R., Kotilainen, J.K., Scarpa, R., Treves, A., Uslenghi, M. 2005, in press (astro-ph/0512328)

[1991] Francis, P.J., Hewett, P.C., Foltz, C.B., et al. 1991 ApJ, 373, 465

[2003] Gebhardt, K., Richstone, D., Tremaine, S., et al. 2003, ApJ, 583, 92

[2003] Heidt, J., Appenzeller, I., Gabasch, A., et al. 2003, A&A, 398, 49

[2004] Jahnke, K., Sanchez, S.F., Wisotzki, L., et al. 2004, ApJ, 614, 568

[1989] Kellermann, K. I.; Sramek, R.; Schmidt, M., Shaffer, D. B., Green, R. 1989, AJ, 98, 1195K

[1996] Kinney, A.L., Calzetti, D., Bohlin, R.C., et al. 1996 ApJ, 467, 38K

[2001] Kormendy, J., & Gebhardt, K. 2001, in AIP Conf. Proc. 586: 20th Texas Symposium on Relativistic Astrophysics, ed J.C. Wheeler & H. Martel (New York: AIP), 363

[2001] Kukula, M.J., Dunlop, J.S., McLure, R.J., et al. 2001, MNRAS, 326, 1533

[2006] Letawe, G., Magain, P., Courbin, F., et al. 2006, in press (astro-ph/0605288)

[2003] Marconi, A., & Hunt, L.K. 2003, ApJ, 589, L21

[2001] McLure, R.J., & Dunlop, J.S. 2002, MNRAS, 331, 795

[2005] Nandra, K., Laird, E.S., Steidel, C.C. 2005, MNRAS, 360L, 39N

[1999] Nilsson, K., Pursimo, T., Takalo, L.O., Sillanpää, A. et al. 1999, PASP, 111, 1223

[2004] Noll, S., Mehlert, D., Appenzeller, I., et al. 2004, A&A, 418, 885

[2006] Novak, G.S., Faber, S.M., Dekel, A. 2006, ApJ, 637, 96

[2001] Percival, W.J., Miller, L., McLure, R.J., Dunlop, J.S. 2001, MNRAS, 322, 843

[1997] Poggianti, B.M. 1997, A&AS, 122, 399

[2001] Ridgway, S.E., Heckman, M., Calzetti, D., Lehnert, M. 2001, ApJ, 550, 122